CANCER

Targeting PSMD14 combined with arachidonic acid induces synthetic lethality via FADS1 m^{6}A modification in triple-negative breast cancer

Yuanhang Yu[1,2]†, Jin Hu[3]†, Wenwen Wang[4]†, Hao Lei[5], Zihan Xi[1], Peiyi Zhang[2], Ende Zhao[6], Chong Lu[1]*, Hengyu Chen[5]*, Chunping Liu[1]*, Lei Li[1]*

Dysregulation of deubiquitination is essential for cancer growth. However, the role of 26*S* proteasome non-ATPase regulatory subunit 14 (PSMD14) in the progression of triple-negative breast cancer (TNBC) remains to be determined. Gain- and loss-of-function experiments showed that silencing PSMD14 notably attenuated the growth, invasion, and metastasis of TNBC cells in vitro and in vivo. Overexpression of PSMD14 produced the opposite results. Mechanistically, PSMD14 decreased K63-linked ubiquitination on SF3B4 protein to de-ubiquitin and stabilize SF3B4 protein. Then, SF3B4/HNRNPC complex bound to FADS1 mRNA and promoted exon inclusion in the target mRNA through m^{6}A site on FADS1 mRNA recognized by HNRNPC, thereby up-regulating the expression of FADS1 and activating Akt/mTOR signaling. Exogenous arachidonic acid supplementation combined with PSMD14 knockdown induced synthetic lethality, which was further confirmed in TNBC organoid (PDO) and TNBC patient-derived xenograft (PDX) mouse models. Overall, our findings reveal an oncogenic role of PSMD14 in TNBC progression, which indicates a potential biomarker and ferroptosis-mediated therapeutic strategy for TNBC.

INTRODUCTION

Breast cancer has the highest incidence rate of any malignancy in women and is the second leading cause of cancer-related death in the world (*1*). Published reports showed that the estimated new cases of breast cancer were 287,850 (31%) and its estimated deaths account for 15% of new cases of breast cancer in 2022 (*1*). Triple-negative breast cancer (TNBC) has the worst prognosis and overall survival (OS) among all the subtypes of breast cancer (*2*). Hence, further elucidating the potential molecular mechanisms associated with TNBC progression is of great significance.

Deubiquitination is considered to play key roles in maintaining cellular homeostasis and proper functions (*3*). Deubiquitinating enzyme (DUB) 26*S* proteasome non–adenosine triphosphatase regulatory subunit 14 (PSMD14), also known as RPN11 and POH1, is one of essential components of 19*S* proteasomal subunit (*4*). Through regulating protein deubiquitination and stabilization, PSMD14 is implicated in various biological processes, including differentiation (*5*), cell viability (*6*), pluripotency (*7*), autophagy (*8*), DNA break responses (*9*), and tumor progression (*10*). Recently, overexpression of PSMD14 was reported in several kinds of human cancers, such as hepatocellular carcinoma (HCC), multiple myeloma, esophageal squamous cell carcinoma, and breast cancer (BC), where it was associated with poor clinical outcomes in patients (*6*, *11*–*13*). PSMD14 acts as an oncogene that promotes tumor progression by deubiquitinating different protein substrates.

N6 methyladenosine (m^{6}A) is a common modification of eukaryotic RNA, referring to the methylation modification of the sixth nitrogen atoms of the RNA molecule adenine (*14*). It is involved in mRNA transcription, processing, translation, and degradation; cell development and differentiation; as well as tumor progression (*15*). M^{6}A modifications can be dynamically regulated, and the modified segments deposited by m^{6}A methyltransferases (writers), removed by m^{6}A demethylases (erasers), and recognized by m^{6}A-binding proteins (readers) dictate the fate of mRNA by modulating their splicing, translation, or stability (*15*). Noteworthy, the biological function of m^{6}A modification mechanism of alternative splicing plays an important role in tumor progression (*16*). HNRNPC, a member of the heterogeneous nuclear ribonucleoproteins, also known as a "reader" of the m^{6}A modification, regulates nonspecific RNA export of RNA splicing sequences, RNA expression, and RNA stability (*17*) and plays an important role in a variety of cancers including breast cancer (*18*–*20*). However, the potential mechanism of HNRNPC in the progression of TNBC needs further exploration.

Ferroptosis is an iron-dependent non-apoptotic cell death process that is a targeted susceptibility to certain cancers (*21*). Lipid peroxidation is the basic mechanism of ferroptosis (*22*). Polyunsaturated fatty acids (PUFAs) are frequently oxidized by lipoxygenases, whose biosynthetic pathway plays a crucial role in the process of ferroptosis in cancer cells (*23*). Meanwhile, it has been reported that fatty acid desaturase-1 (FADS1), as a key rate-limiting enzyme in the metabolism of PUFAs (*24*), converts dihomo-γ-linoleic acid (DGLA) into arachidonic acid (AA), and thus plays an important role in mediating ferroptosis.

In this study, we evaluated the oncogenic role of PSMD14 in TNBC malignancy using multiple in vitro and in vivo models. Furthermore, pulldown, mass spectrum, and co-immunoprecipitation

[1]Department of Breast and Thyroid Surgery, Union Hospital, Tongji Medical College, Huazhong University of Science and Technology, Wuhan 430022, China. [2]Cancer Center, Union Hospital, Tongji Medical College, Huazhong University of Science and Technology, Wuhan, Hubei 430022, China. [3]Department of Breast and Thyroid Surgery, Renmin Hospital of Wuhan University, Wuhan 430060, China. [4]Department of Gynecology and Obstetrics, Union Hospital, Tongji Medical College, Huazhong University of Science and Technology, Wuhan 430022, China. [5]Department of Breast and Thyroid Surgery, The Second Affiliated Hospital of Hainan Medical University and Key Laboratory of Tropical Translational Medicine of Ministry of Education and School of Tropical Medicine, Hainan Medical University, Haikou 570311, China. [6]Department of Gastrointestinal Surgery, Union Hospital, Tongji Medical College, Huazhong University of Science and Technology, Wuhan 430022, China.
*Corresponding author. Email: leili2008@hust.edu.cn (L.L.); lcp191@163.com (C. Liu); chenhy9012@163.com (H.C.); lcwhxh@hust.edu.cn (C. Lu)
†These authors contributed equally to this work.

(Co-IP) assays were performed to validate the PSMD14/SF3B4/HNRNPC/FADS1 signaling axis, which aggravates the progression of breast cancer by activating the Akt/mTOR pathway. After PSMD14 knockdown, the expression of FADS1 and the production of unsaturated fatty acids decreased, thus reducing the sensitivity to ferroptosis. Therefore, exogenous AA supplementation combined with PSMD14 deletion induced the synthetic lethality of TNBC, which was verified in patient-derived xenograft (PDX)/patient-derived organoid (PDO) models. Together, our study suggests a potential prognostic biomarker and therapeutic target for patients with TNBC.

RESULTS

PSMD14 is highly expressed and is associated with poor prognosis in TNBC

The expression of PSMD14 were assessed by GEPIA (http://gepia.cancer-pku.cn/) based on high-throughput RNA-sequencing (RNA-seq) data of BC cohort of the The Cancer Genome Atlas (TCGA) database. Results showed that the expression level of PSMD14 was notably up-regulated in BC samples compared with that in nonmalignant samples (Fig. 1A). We then verified the PSMD14 mRNA and protein expression and found that the mRNA level of PSMD14 was enhanced in 65 pairs of TNBC tissues than that in paired adjacent normal breast tissues by reverse transcription quantitative polymerase chain reaction (RT-qPCR) and Western blotting (Fig. 1, B and C). The expression of PSMD14 was markedly higher in TNBC cells (MDA-MB-231, HCC1937, BT20, and BT-549) than in normal breast epithelial cells MCF-10A (Fig. 1, D and E). In addition, paraffin specimens from 28 pairs of TNBC tissues and paired adjacent normal breast tissues were used to perform immunohistochemical (IHC) detection. Results indicated that the average expression level of PSMD14 in TNBC group was notably higher than that in paired adjacent normal breast tissues group ($P < 0.05$) (Fig. 1F and fig. S1A). Patients with breast cancer and high PSMD14 mRNA levels had poorer disease-free survival and OS than those with low expression (Fig. 1, G and H). In addition, patients with TNBC and high PSMD14 protein levels had poorer recurrence-free survival and distant metastasis–free survival than those with low expression (Fig. 1, I and J).

Subsequently, the correlation between PSMD14 expression levels and clinicopathological features of patients with TNBC was analyzed using 51 pairs of cancerous tissue samples and adjacent normal tissue samples. The results indicated that the high expression level of PSMD14 was positively associated with TNM stage, lymph node metastasis, differentiation, and Ki-67 expression in patients with TNBC (table S3). Collectively, these results demonstrated that PSMD14 exerted an oncogenic role in the aggressiveness of TNBC.

PSMD14 promotes the proliferation, migration, and invasion of TNBC cells

To investigate the biological role of PSMD14 in TNBC, pLKO.1 short hairpin (sh)–PSMD14 1/2/3 and vector were used to knockdown the expression of PSMD14 in TNBC cells, and the knockdown efficiency were examined by RT-qPCR and Weston blot (fig. S1B). Cell counting kit–8 (CCK-8) (Fig. 2, A and B), 5-ethynyl-2′-deoxyuridine (EdU) (Fig. 2E and fig. S1D), and colony formation (Fig. 2G) assay results demonstrated that silencing of PSMD14 notability repressed the proliferation and colony formation of cells compared to the control groups in MDA-MB-231 and BT-549 cells. Furthermore, both wound-healing (Fig. 2I and fig. S1F) and transwell assays (Fig. 2, K and M) indicated that PSMD14 depletion exhibited less aggressive migratory and invasive potential.

We further confirmed the tumor-promoting effect of PSMD14 by transfecting BT-549 and HCC1937 cells with a lentiviral vector containing the PSMD14 sequence or vector control, and the overexpression efficiency was examined by RT-qPCR (fig. S1C). The results showed that overexpression of PSMD14 increased the proliferation ability of the BT-549 and HCC1937 cells (Fig. 2, C, D, F, and H, and fig. S1E). Moreover, the migration and invasion capacity of TNBC cells were markedly increased after PSMD14 overexpression (Fig. 2, J, L, and N, and fig. S1G).

PSMD14 interacts with HNRNPC and SF3B4 proteins in TNBC cells

To explore the underlying molecular mechanism of PSMD14 in TNBC progression, we expressed hemagglutinin (HA)–tagged PSMD14 in MDA-MB-231 cells and carried out immunoaffinity purification of HA-PSMD14 and its associated proteins. A representative silver staining gel of purified HA-PSMD14. The results showed that two obvious protein bands could be observed between 40 and 55kDa in the group with HA-PSMD14 beads, but this protein band was found much weaker in group with control beads (Fig. 3A and fig. S2A). The band in the gel was excised and identified by liquid chromatography–tandem mass spectrometry (LC-MS/MS). A Venn diagram revealed nine candidate binding proteins (STX10, PTBP3, SF3B4, POP7, PKP3, NDUFS8, FABP5, HIGD2A, and HNRNPC) in MDA-MB-231 and BT549 cells (Fig. 3B and tables S4 and S5). Identification of the peptides implied that the PSMD14-protein complex most likely represented HNRNPC and SF3B4 in the ranked list of recognized proteins (Fig. 3, C and D, and fig. S2, B and C), which was verified by subsequent Western blot assay (Fig. 3E and fig. S2D). To further verify the interaction between PSMD14 and HNRNPC/SF3B4, we confirmed the co-localization of endogenously expressed PSDM14, HNRNPC, and SF3B4 in the nucleus by immunofluorescence in situ hybridization analysis (Fig. 3, F and G). Next, the expression levels of HNRNPC and SF3B4 in TNBC tumor tissues and corresponding normal tissues were detected by IHC assays (Fig. 3, H and I). Compared with corresponding normal tissues, the IHC scores of HNRNPC and SF3B were higher in TNBC tissue samples (Fig. 3, J and K). Pearson correlation analysis demonstrated that HNRNPC and SF3B expression was positively associated with the levels of PSMD14 in the TNBC samples (Fig. 3, L and M). On the basis of these results, it can be concluded that PSMD14 exerts its carcinogenic effect through binding with the proteins HNRNPC and SF3B4.

PSMD14 maintains SF3B4 protein stability by decreasing its ubiquitination

Whether HNRNPC and SF3B4 can both be deubiquitinated by PSMD14 could be further studied. No change was found in the mRNA or protein level of HNRNPC, as far as in the mRNA level of SF3B4, while this protein band was weaker after suppressing PSMD14 expression (Fig. 4A). Given that PSMD14 was a deubiquitinating enzyme, we wondered whether PSMD14 regulated deubiquitylation. Co-IP experiment was performed in MDA-MB-231 and BT-549 cells. As expected, PSMD14 notably reduced SF3B4 ubiquitination (Fig. 4B), while SF3B4 ubiquitination was elevated after PSMD14 down-regulated (Fig. 4C). PSMD14 down-regulation induced proteasome degradation of SF3B4 (Fig. 4D). PSMD14

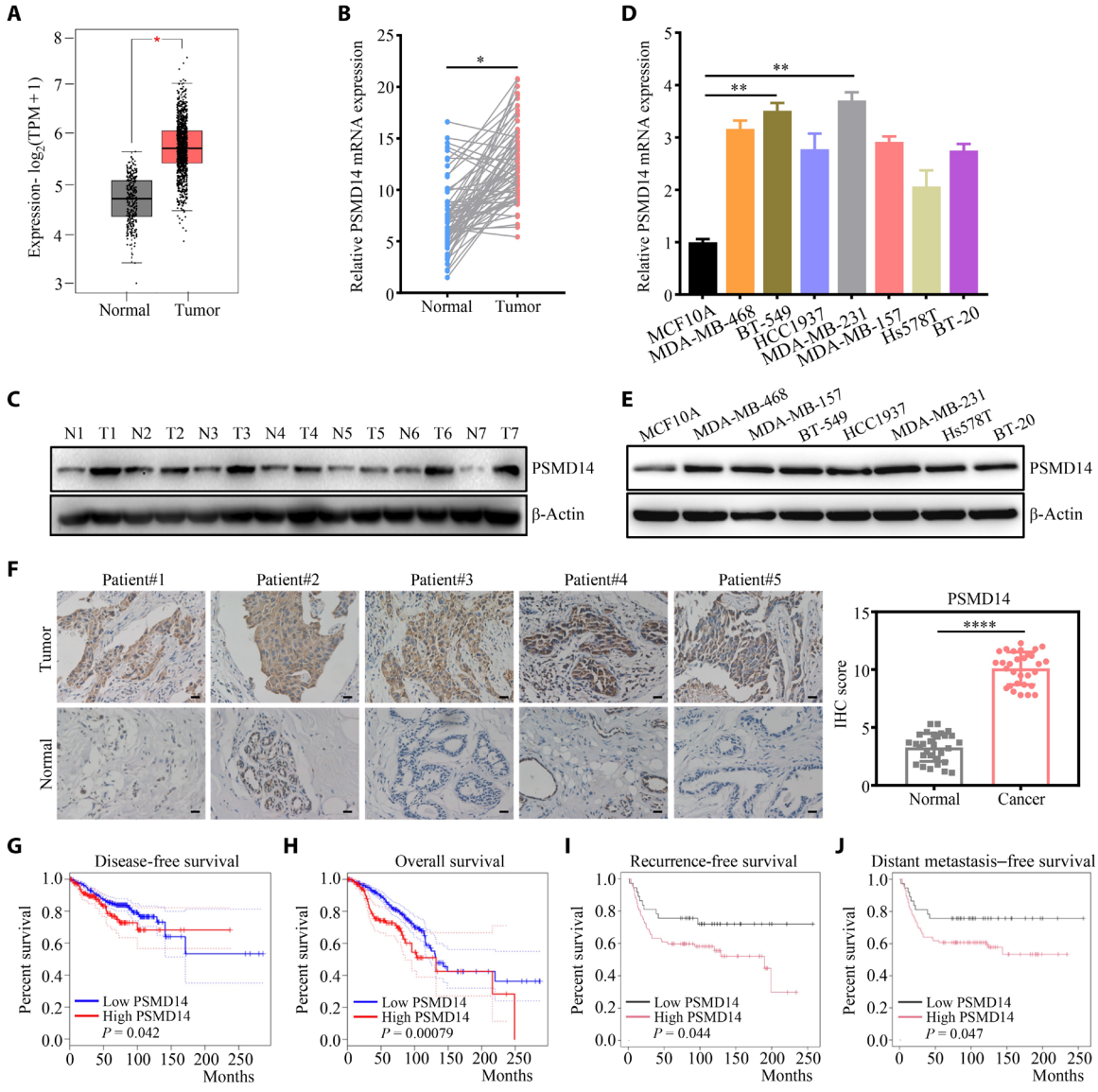

Fig. 1. PSMD14 is up-regulated in TNBC and is associated with poor prognosis. (**A**) The block diagram shows the mRNA level of PSMD14 in BC tissues and noncancerous tissues in TCGA datasets from GEPIA (**B**) Reverse transcription quantitative polymerase chain reaction (RT-qPCR) analysis of PSMD14 mRNA expression level in 65 pairs of TNBC tissues and adjacent normal tissues. (**C**) Western blotting analysis of PSMD14 protein expression level in seven pairs of TNBC tissues and adjacent normal tissues. (**D** and **E**) RT-qPCR (D) and Western blotting (E) of the expression levels of PSMD14 in normal breast cell line and breast cancer cell lines, respectively. (**F**) Representative immunohistochemical (IHC) staining images showing PSMD14 expression (left) and IHC scores of PSMD14 (right) in 28 pairs of TNBC and adjacent normal tissues. Scale bars, 20 μm. (**G** and **H**) Kaplan-Meier analysis of disease-free survival (G) and overall survival (OS) (H) in the TCGA dataset of all patients with breast cancer with high or low PSDM14 mRNA expression. (**I** and **J**) Kaplan-Meier analysis of recurrence-free survival (I) and distant metastasis–free survival (J) of patients with TNBC and high or low PSDM14 protein expression.

down-regulation reduced SF3B4 protein half-life, but PSMD14 overexpression elevated SF3B4 stability after using cycloheximide (CHX) to inhibit protein synthesis (Fig. 4, E and F). Subsequently, to determine whether the DUB activity of PSMD14 is necessary for the stability of the SF3B4 protein, the histidine at residue 113 and the cysteine at residue 120 of PSMD14 were replaced with glutamic acid and serine, respectively, to produce HA-PSMD14-ΔH113Q and HA-PSMD14-ΔC120S. The PSMD14 mutants with impaired deubiquitinase activity, i.e., HA-PSMD14-ΔH113Q and HA-PSMD14-ΔC120S, did not deubiquitinate the Flag-SF3B4 as much as wild-type PSMD14 (Fig. 4G). To identify which polyubiquitination pattern of SF3B4 is deubiquitinated by PSMD14, wild-type ubiquitin (His-Ub), the K63 ubiquitin mutant (His-Ub-K63) in which only lysine 63 is left intact, and the K48 ubiquitin mutant (His-Ub-K48) in which six lysine residues except for lysine 48 are substituted into arginines were transfected into MDA-MB-231 cells with or without HA-PSMD14. When the plasmid encoding the His-Ub-K63 mutant was transfected with the indicated combinations, cells were pretreated with MG132 for 8 hours to prevent proteasomal degradation of Flag-SF3B4. The K63-linked polyubiquitination of the SF3B4 protein was notably deubiquitinated by PSMD14 (Fig. 4H).

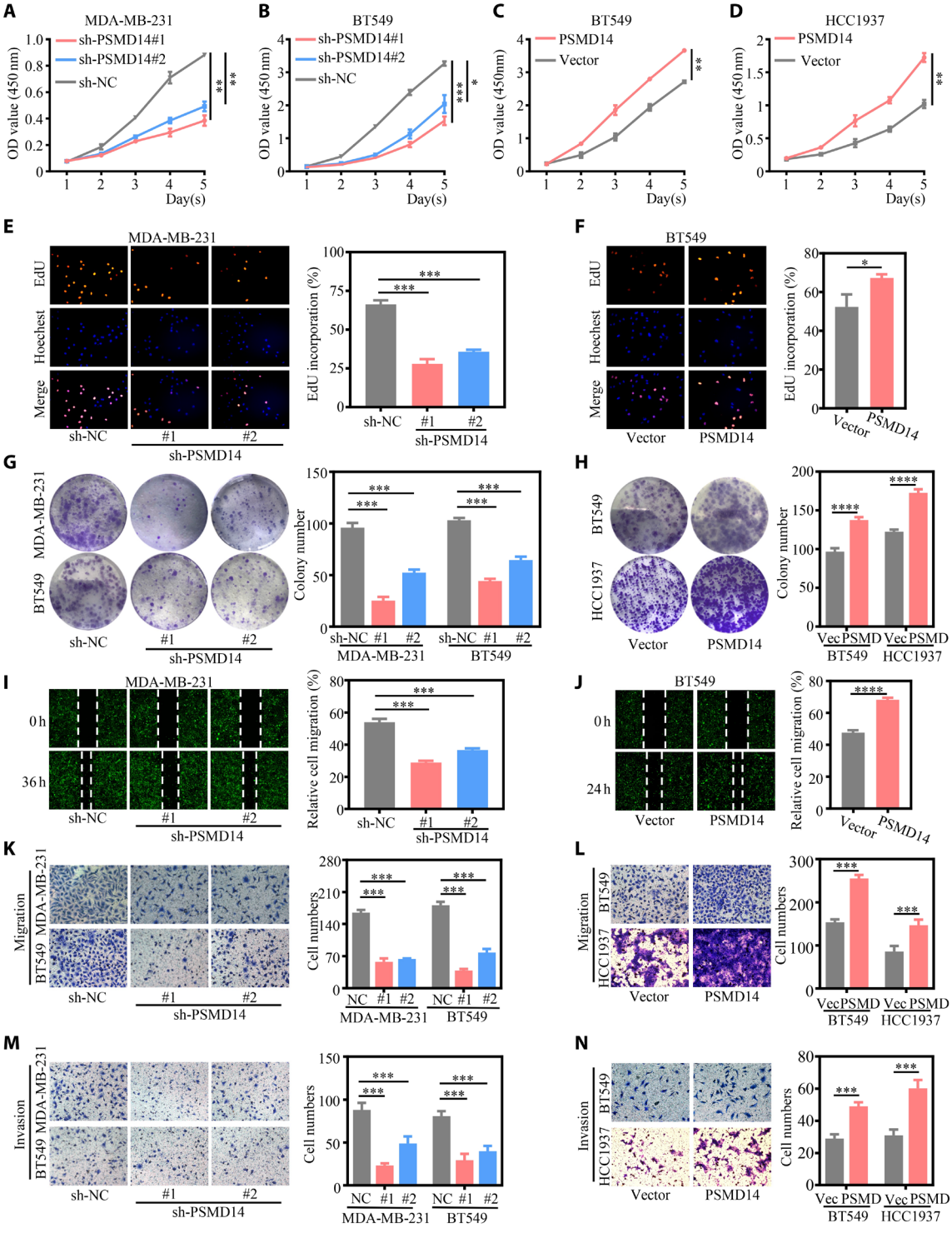

Fig. 2. PSMD14 inhibits proliferation, migration, and invasion of TNBC cells in vitro. (**A** and **B**) Cell growth after PSMD14 knockdown in MDA-MB-231 (A) and BT549 (B) cells as shown by cell counting kit–8 (CCK-8) assays. OD, optical density. (**C** and **D**) Cell growth after PSMD14 overexpression in BT549 (C) and HCC1937 (D) cells as determined by CCK-8 assays. (**E** and **F**) Cell growth after PSMD14 knockdown in MDA-MB-231 (E) and PSMD14 overexpression BT549 (F) cells as shown by EdU assays, respectively. Representative images are shown in the left panel, and quantification of EdU positive cells are shown in the right panel. (**G** and **H**) Cell growth after PSMD14-knockdown MDA-MB-231 and BT549 cells (G), and PSMD14-overexpressing BT549 and HCC1937 cells (H) as determined by colony formation assays, respectively. (**I** and **J**) Effects of PSMD14 on migration abilities of PSMD14-knockdown MDA-MB-231 (I) and PSMD14-overexpressing BT549 (J) cells as determined by wound-healing assays, respectively. h, hours. (**K** to **N**) Effects of PSMD14 on migration and invasive abilities of PSMD14-knockdown MDA-MB-231 and BT549 cells, and PSMD14-overexpressing BT549 and HCC1937 cells as determined by transwell invasion assays, respectively.

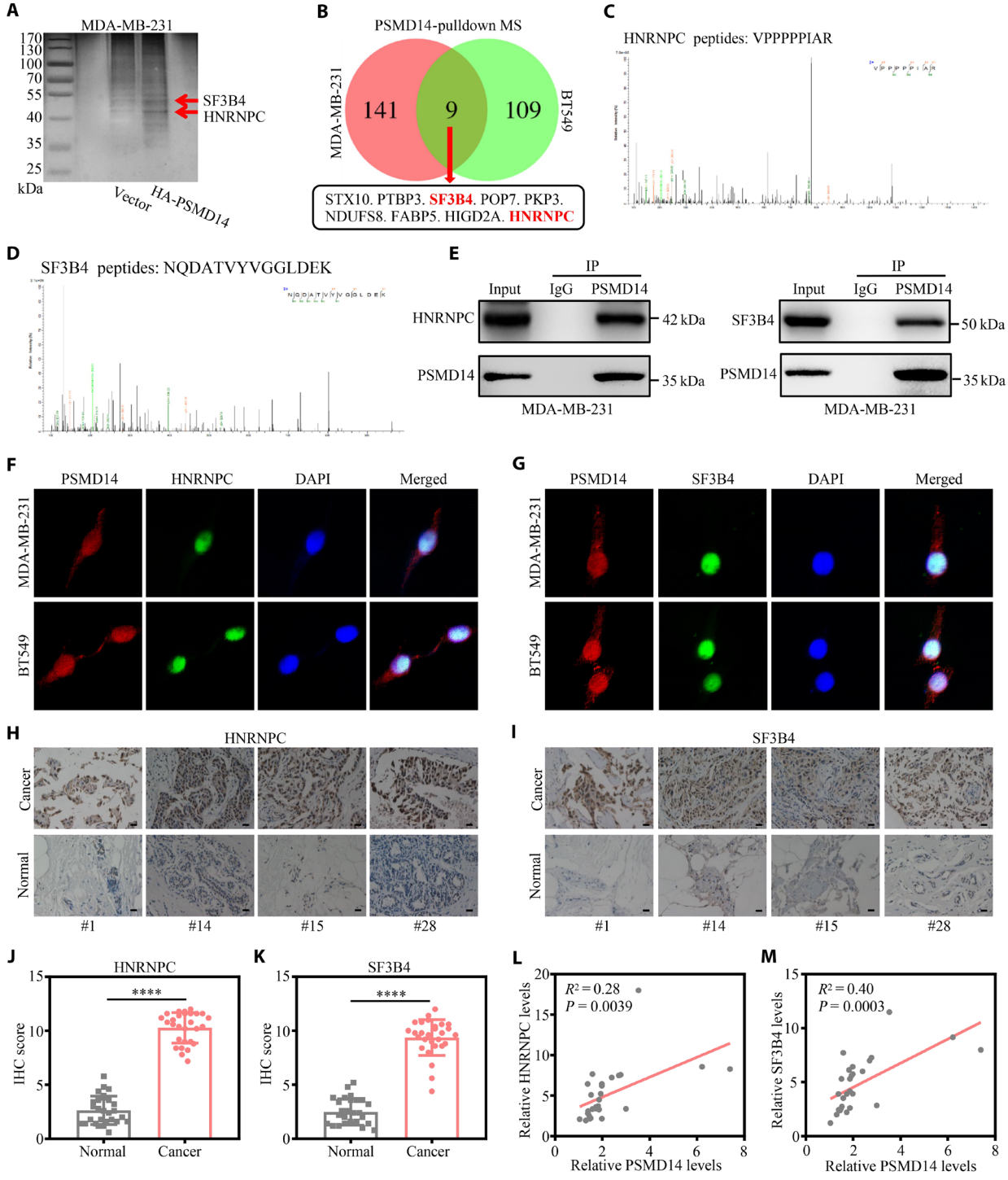

Fig. 3. PSMD14 binds to HNRNPC and SF3B4 protein. (**A**) Silver stain showing proteins that immunoprecipitated (IP) with HA-PSMD14. (**B**) Venn diagram indicating the discovery of proteins interacting with PSMD14 that were found in MDA-MB-231 and BT549 cells. (**C**) Mass spectrometry assay depicted the HNRNPC peptides pulled down by anti-PSMD14 antibody in MDA-MB-231 cell. (**D**) Mass spectrometry assay depicted the SF3B4 peptides pulled down by anti-PSMD14 antibody in MDA-MB-231 cells. (**E**) IP assay verified the combinations between PSMD14 and HNRNPC and between PSMD14 and SF3B4 in MDA-MB-231 cells. IgG, immunoglobulin G. (**F**) The co-localization status of PSMD14 (red) and HNRNPC (green) in MDA-MB-231, and BT549 cells was reflected by immunofluorescence (IF) assay. (**G**) The co-localization status of PSMD14 (red) and SF3B4 (green) in MDA-MB-231 and BT549 cells was reflected by IF assay. (**H**) Representative IHC images of HNRNPC in TNBC tumor tissues and corresponding normal tissues. Scale bars, 20 μm. DAPI, 4′,6-diamidino-2-phenylindole. (**I**) Representative IHC images of SF3B4 in TNBC tumor tissues and corresponding normal tissues. Scale bars, 20 μm. (**J**) IHC score of HNRNPC in 28 pairs of TNBC tumor tissues and corresponding normal tissues. (**K**) IHC score of SF3B4 in 28 pairs of TNBC tumor tissues and corresponding normal tissues. (**L**) Pearson correlation analysis showed that the expression of HNRNPC was positively correlated with the level of PSMD14. (**M**) Pearson correlation analysis showed that the expression of SF3B4 was positively correlated with the level of PSMD14. R^2, coefficient of determination.

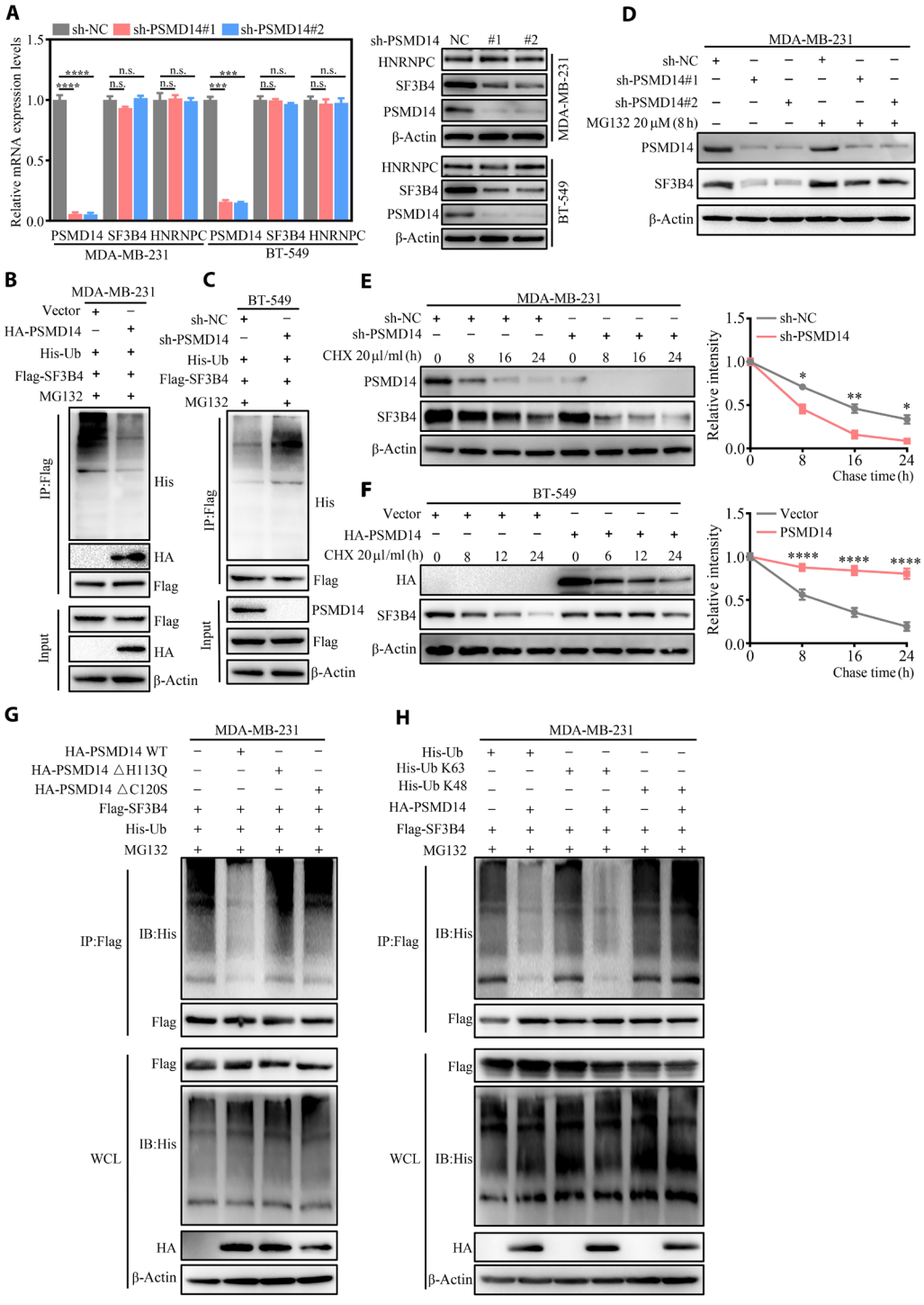

Fig. 4. PSMD14 maintains SF3B4 protein stability by decreasing its ubiquitination. (**A**) The level of HNRNPC and SF3B4 were tested in the mRNA and protein level. n.s., not significant. (**B**) MDA-MB-231 cells were transfected with indicated constructs. The impact of PSMD14 overexpression on SF3B4 ubiquitination was tested. (**C**) SF3B4 ubiquitination was conducted upon PSMD14 depletion. (**D**) Western blotting analysis of PSMD14 and SF3B4 in MDA-MB-231 cells transfected with the indicated plasmids with or without MG132 (26*S* proteasome inhibitor, 20 μM, 8 hours). (**E**) MDA-MB-231 cells were transfected with control (sh-NC) or sh-PSMD14 for 24 hours followed by CHX (20 μg/ml) for indicated time. Cells were immunoblotted with anti-SF3B4 and anti-PSMD14 antibodies. (**F**) MDA-MB-231 cells were transfected with pcDNA3.1 empty vector or pcDNA3.1-HA-PSMD14 plasmid for 24 hours followed by CHX (20 μg/ml) for indicated time. Cells were immunoblotted with anti-SF3B4 and anti-PSMD14 antibodies. (**G**) The catalytically inactive DUB mutant of HA-PSMD14 (H113Q, C120A, or C120S) and wild-type HA-PSMD14 were co-transfected into MDA-MB-231 cells with Flag-SF3B4, His-Ub, and MG132 in the indicated combinations. (**H**) Flag-ALK2 and HA-PSMD14 were co-transfected into human embryonic kidney 293FT cells with a plasmid encoding wild-type or lysine mutant (K48 or K63) HA-Ub in the indicated combinations. When the K48 mutant of His-Ub was transfected, MG132 was treated to prevent SF3B4 degradation. IB, immunoblotting. WCL, whole cell lysate. h, hours.

Abnormal RNA splicing of FADS1 mediated by the m^{6}A modification pathway

To expound the potential functional mechanism of PSMD14 in TNBC progression, we analyzed the aberrant transcriptome profile in MDA-MB-231 cells transfected with sh-PSMD14 using RNA-seq. The results showed that there were 222 genes distinctly up-regulated and 988 genes that were down-regulated after PSMD14 ablation (fold change ≥ 1.5, $P < 0.05$) (Fig. 5A and table S6). The Gene Ontology functional and Kyoto Encyclopedia of Genes and Genomes pathway enrichment analyses showed that the up-regulation of differentially expressed genes (DEGs) was mainly related to protein binding and alternative splicing (fig. S3, A and B). Subsequently, replicate multivariate analysis of transcript splicing (rMATS) software was then used to perform differential alternative splice event analysis (*25*), and five main alternative splicing (AS) events were analyzed, namely, alternative 3′ splicing sites (A3SSs), alternative 5′ splicing sites (A5SSs), mutually exclusive exons (MXEs), retained introns (RIs), and skipped exons (SEs). Based on a false discovery rate threshold of < 0.05, there were 231 differential splicing genes (DSGs) with A3SSs, 132 DSGs with A5SSs, 632 DSGs with MXEs, 39 DSGs with RIs, and 2906 DSGs with SEs (Fig. 5B). Studies have shown that reader protein plays an important role in alternative splicing through m^{6}A modification pathway (*26*), and HNRNPC, as a reader protein, mediates alternative splicing of target genes (*27*). Meanwhile, the study showed that reader protein can function as a recruiter of mRNA splicing factors and promote exon inclusion of target mRNA consistent with splicing factor (*28*). Therefore, HNRNPC may promote exon inclusion consistent with SF3B4 via m^{6}A modification pathway, and potential physical interaction between HNRNPC and SF3B4 proteins was detected. Co-IP experiments using lysates from 293T cells co-transfected with Myc-HNRNPC and FLAG-SF3B4 demonstrated that exogenously expressed SF3B4 or HNRNPC can be pulled down with Myc-HNRNPC or FLAG-SF3B4, respectively (fig. S3, E and F). To further validate this finding, FLAG-HNRNPC or FLAG-SF3B4 were expressed in 293T cells and immunoprecipitated with anti-FLAG beads. Endogenous SF3B4 and HNRNPC were then tested in the immunoprecipitated protein complex using antibodies against SF3B4 and HNRNPC. Consistently, endogenous SF3B4 or HNRNPC can be pulled down with FLAG-HNRNPC or FLAG-SF3B4, respectively (fig. S3, G and H), supporting a potential direct interaction between HNRNPC and SF3B4 as well as the regulation of alternative splicing by HNRNPC via m^{6}A modification. Then, the target genes analysis of PSMD14 by using a Venn diagram in AS event different genes, HNRNPC perturbated down-regulated genes via m^{6}A modification, and sh-PSMD14 down-regulated genes, identified eight candidate proteins (FADS1, CEP290, TMEM116, IQCH, FANCD2, SLC4A7, TMEM68, and AC007264.3), of which the expression difference of FADS1 was the most notable (Fig. 5, C and D). RT-qPCR analysis revealed that PSMD14 depletion conspicuously decreased the FADS1 level in TNBC cells (Fig. 5E and fig. S3C). Western blot analysis further demonstrated that FADS1 was positively regulated by PSMD14 in TNBC cells (Fig. 5F and fig. S3D). Meanwhile, the exon inclusion levels of FADS1 mRNA was then compared between sh-PSMD14 and control groups through the rMATS software, indicating that depletion of PSMD14 reduced the inclusion of exon 10 on FADS1 mRNA (Fig. 5, G to I). Meanwhile, paraffin specimens from 28 pairs of TNBC tissues and paired adjacent normal breast tissues were used to perform IHC detection. Results indicated that the average expression level of FADS1 in TNBC group was higher than that in paired adjacent normal breast tissues group ($P < 0.05$) (Fig. 5J and fig. S3O). Moreover, the splicing pattern of FADS1 exon 10 upon individual knockdown of PSMD14, SF3B4, or HENRPC was validated. Consistent exon-splicing patterns with endogenous FADS1 exon 10 were observed (Fig. 5K and fig. S3I). Furthermore, Northern blotting was used to detect differences in mRNA size. The splicing patterns of FADS1 exon 10 following the separate knockdown of PSMD14, SF3B4, or HENRPC were also validated by the Northern blotting (fig. S3J). RNA binding protein immunoprecipitation (RIP) assays further validated the interaction between SF3B4 and FADS1 mRNA in MDA-MB-231 and BT549 cells (Fig. 5L). To verify the important role of m^{6}A in mediating splicing events, methylated RNA immunoprecipitation (MeRIP)–qPCR was used to reveal that PSMD14 depletion notably attenuated the expression of m^{6}A in FADS1 exon 10 mRNA (Fig. 5M and fig. S3K). However, the expression of the m^{6}A sites, including those in exons 9 and 11, had no difference between the PSMD14 silencing group and the control group (fig. S3, L to N). We used the m^{6}A probe with an RNA-pulldown assay to show that HNRNPC, as an m^{6}A reader, bound with m^{6}A-methylating FADS1 mRNA. Similar results were also observed with SF3B4 (Fig. 5N).

In addition, whether the interaction between SF3B4/HNRNPC and FADS1 mRNA is m^{6}A dependent was further investigated. The short hairpin RNA (shRNA) FADS1-knockdown efficiency was confirmed by Western blot (fig. S4A). The wild-type and exogenous mutant plasmids at m^{6}A modification site in exon 10 of FADS1 mRNA (Mut-m^{6}A-Exo) were transfected into TNBC cells with FADS1 knockdown, respectively. RIP assay results showed that the mutant m^{6}A modification site attenuate the interaction between SF3B4 and FADS1 mRNA (fig. S4B). Meanwhile, the role of the m^{6}A modification site on exon 10 of FADS1 mRNA in the splicing and quantity of FADS1 mRNA was further explored, and exogenous mutant and wild-type plasmids at the m^{6}A modification site of FADS1 exon 10 were transfected into TNBC cells that notably knocked down FADS1. The results of PCR and gel electrophoresis demonstrated that the mutation at the FADS1 exon 10 m^{6}A modification site promoted the splicing of FADS1 mRNA, leading to reduced expression (fig. S4, C and D). Furthermore, we used CRISPR-Cas9 to introduce an endogenous A-to-G mutation in the m^{6}A region of FADS1 exon 10 in MDA-MB-231 cells (fig. S4, E and F). Subsequently, PCR, gel electrophoresis, and Northern blot (NB) analysis were used to detect changes in FADS1 mRNA splicing and quantity. The results showed that the endogenous mutation at the FADS1 exon 10 m^{6}A modification site promoted FADS1 mRNA splicing, but knockdown of HNRNPC or SF3B4 did not promote FADS1 mRNA splicing in cells with endogenous mutations at the FADS1 exon 10 m^{6}A modification site (Fig. 5O and fig. S4G). Together, these results indicated that HNRNPC consistent with SF3B4 binding to m^{6}A-modified site on FADS1 exon 10 and promoting exon inclusion, so PSMD14 silencing lead to SF3B4 degradation and facilitated skipping.

FADS1 is a functional downstream mediator of PSMD14

The above results indicate that PSMD14 can regulate the expression of FADS1 and thereby act as an oncogene. PSMD14-shRNA alone or PSMD14-shRNA combined with FADS1-overexpressing plasmids were transfected into MDA-MB-231 and BT-549 cells to further determine whether FADS1 is a functional downstream mediator of PSMD14 in TNBC cells. The results of biological function assays showed that PSMD14 silencing markedly decreased proliferation,

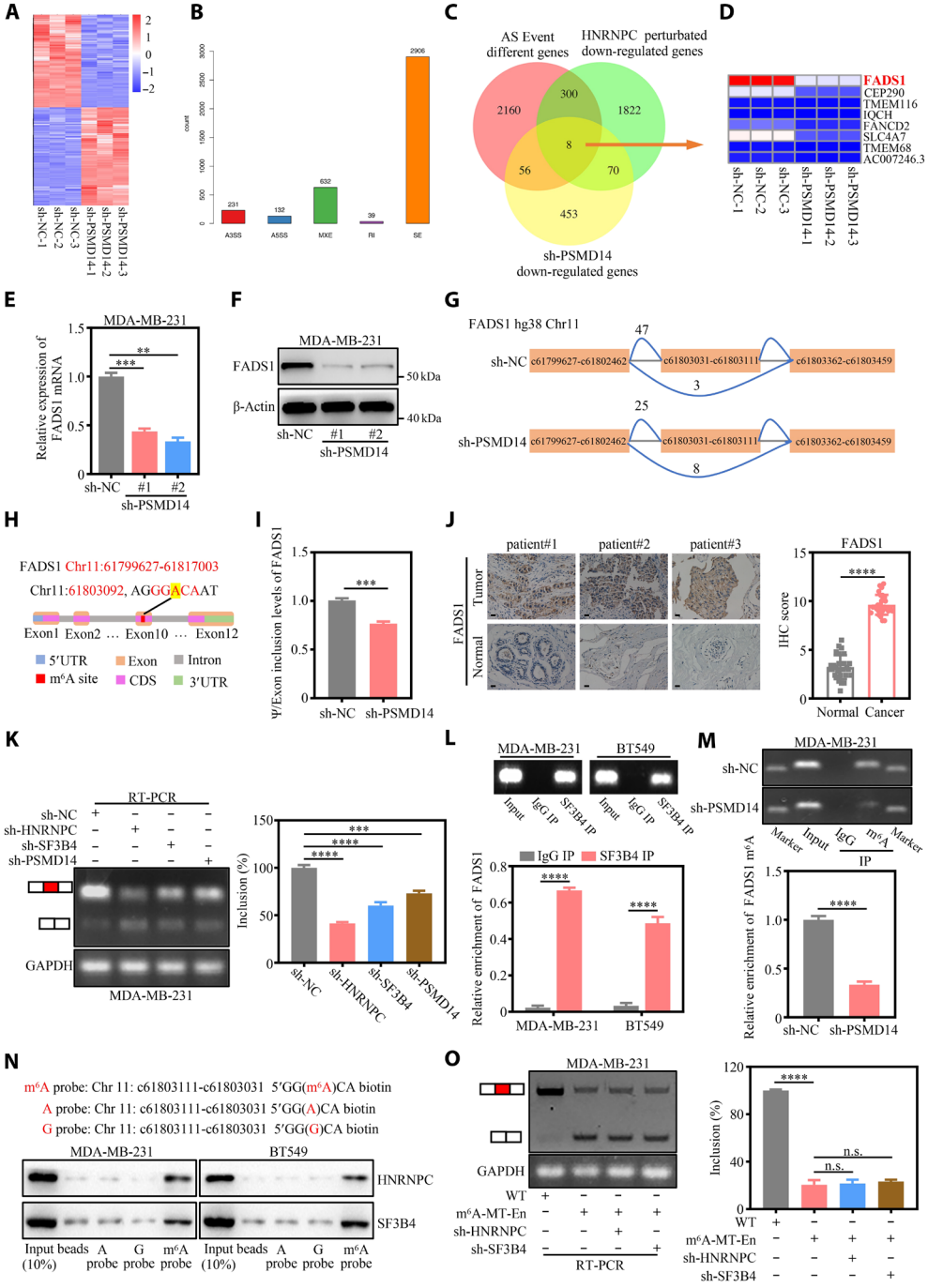

Fig. 5. PSMD14 drives aberrant RNA splicing of FADS1 via m^{6}A modification. (**A**) DEGs identified by RNA-seq that sh-PSMD14 lentiviruses or control in MDA-MB-231 cells are presented in the heatmap. (**B**) Types of alternative splicing events that occur upon PSMD14 knockdown. (**C**) Venn diagram illustrating the overlap between DEGs obtained by RNA-seq, PSMD14-regulated splicing events of AS type, and HNRNPC target genes predicted by the m^{6}A database. (**D**) Heatmap listed the DEGs obtained from the intersection of the datasets. (**E**) RT-qPCR analysis of FADS1 mRNA upon PSMD14 knockdown in MDA-MB-231 cells. (**F**) Western blot analysis of FADS1 expression upon PSMD14 knockdown in MDA-MB-231 cells. (**G**) A schematic diagram shows the number of alternative splicing events in exons of FADS1 upon PSMD14 knockdown or control in MDA-MB-231 cells. (**H**) Schematic image of the m^{6}A motif on the FADS1 exon. (**I**) The exon inclusion levels of FADS1 were based on the expression of alternative splicing events (ψ) analyzed by replicate multivariate analysis of transcript splicing (rMATS). 3′UTR, 3′ untranslated region; 5′UTR, 5′ untranslated region. (**J**) Representative IHC images showing FADS1 expression (left) and IHC scores of FADS1 (right) in 28 pairs of TNBC and adjacent normal tissues. Scale bars, 20 μm. (**K**) The inclusion level of exon in FADS1 was validated by RT-PCR in the MDA-MB-231 cells transfected with sh-NC, sh-PSMD14, sh-HNRNPC, and sh-SF3B4. (**L**) RNA binding protein immunoprecipitation (RIP) detection was performed in TNBC cells using SF3B4 and immunoglobulin G (IgG) antibodies. (**M**) Methylated RNA immunoprecipitation (MeRIP)–qPCR was used to quantify relative FADS1 m^{6}A levels in PSMD14 knockdown and control TNBC cells. (**N**) Position of m^{6}A peak in FADS1 mRNA (top), and RNA probe sequences for RNA-pulldown assays (bottom). (**O**) The inclusion level of exon in FADS1 was validated by RT-PCR and gel electrophoresis in the MDA-MB-231 cells mutated at FADS1 exon 10 m^{6}A-specific modification site mediated by CRISPR-Cas9 transfected with sh-HNRNPC or sh-SF3B4, respectively. GAPDH, glyceraldehyde-3-phosphate dehydrogenase; WT, wild type.

migration, and invasiveness, but these effects were reversed in the TNBC cells co-transfected with sh-PSMD14 and FADS1-expressing plasmids (Fig. 6, A to D, and fig. S5, A to D). Meanwhile, study has showed that FADS1, by activating Akt/mTOR signaling, promoted the progression of laryngeal squamous cell carcinoma (*29*). We presumed that PSMD14 might regulate the progression of TNBC via the FADS1/Akt/mTOR pathway. Consistently, Western blot results confirmed that PSMD14 silencing notably decreased the protein expression levels of phosphorylated (p)–Akt and p-mTOR (Fig. 6E and fig. S5E). To further validate our hypothesis, we treated cells with MK-2206, an inhibitor of Akt, to explore the biological effects on TNBC cells. As expected, ectopic expression of FADS1 produced the same results as the overexpression of PSMD14 in TNBC cells. Furthermore, treatment with MK-2206 repressed proliferation, migration, and invasion in BT-549 and HCC1937 cells. However, overexpression of PSMD14 rescued these effects and the protein expression levels of p-Akt and p-mTOR induced by MK-2206 treatment (Fig. 6, F to I, and fig. S5, F to K). In addition, whether the downstream molecular activity of FADS1 is dependent on splicing of FADS1 mRNA regulated by m^6A was further investigated. Western blotting results showed that the expression of activated Akt/mTOR was decreased after mutation of the m^6A modification site of exon 10 (fig. S5, L and M). Overall, the above results implied that, as a functional downstream target of PSMD14, FADS1 mediated the regulatory role of the PSMD14/Akt/mTOR signaling pathway in the malignant progression of TNBC.

PSMD14 knockdown reduces sensitivity to ferroptosis and synthetic lethality with AA supplementation

FADS1 is an enzyme essential for the generation of AA (C20:4) and adrenic acid (AdA; C22:4) from linoleic acid (LA; C18:2) (Fig. 7A). Using liquid chromatography–mass spectrometry (LC-MS) to examine the levels of the lipids in 28 pairs of TNBC tissues and adjacent normal tissues, we found that the DGLA (C20:3) concentration showed no difference (fig. S5A), whereas the concentration of AA and the AA/DGLA ratio were visibly increased in TNBC samples, which was consistent with the high expression of PSMD14/FADS1 in TNBC tissues (fig. S5, B and C). To verify whether PSMD14 was involved in the regulation of lipid metabolism, an LC-MS assay was used to detect metabolites in TNBC cells. As shown in the volcano plot, compared to the control group, AA was decreased in the sh-PSMD14 group (Fig. 7B).

A previous study demonstrated that the resistance to ferroptosis induced by the down-regulation of FADS1 was attributed to the reduction of ferroptosis-related lipids (*23*). We further verified whether PSMD14 was involved in the regulation of ferroptosis. Results from LC-MS as well as cluster analysis based on the heat map revealed that deletion of PSMD14 notably decreased the relative intensity of AA and AdA, for which synthesis was determined by FADS1 (Fig. 7, C and D, and fig. S5M). PSMD14 silencing did not affect the relative intensity of LA and DGLA but decreased the content of phosphatidylethanolamine (fig. S5, D to F). Moreover, by analyzing the cellular viability after treatment with RSL3, which generally causes ferroptosis-induced cell death and reactive oxygen species (ROS) accumulation, we found that sh-PSMD14 substantially reduced the sensitivity of MDA-MB-231 and BT-549 cells to RSL3 (fig. S5, G and H). Meanwhile, we performed C11 BODIPY 581/591 staining to measure the levels of lipid peroxidation, a hallmark of ferroptosis (*30*), and the results showed that compared with the control group, PSMD14 deficiency are highly resistant to RSL3-induced ferroptosis by suppressing lipid peroxidation (fig. S5, I and J), and reduced the cytotoxicity induced by RSL3 in TNBC cells (fig. S5, K and L). Coincidentally, compared with the control group that was supplemented with exogenous AA, additional AA combined with PSMD14 knockdown distinctly promoted the sensitivity to RSL3 (Fig. 7, E and F) and enhanced the cytotoxicity induced by RSL3 in TNBC (Fig. 7, G and H). Furthermore, additional AA supplementation restored the RSL3-induced lipid peroxidation and ROS accumulation decrease caused by PSMD14 deficiency (Fig. 7, I to L).

Furthermore, to test the effect of this specific modification in mediating the targeting PSMD14 plus AA that induces the synthetic lethality, we used CRISPR-Cas9 to generate knock-in cells with the TNBC cell line MDA-MB-231, introducing an A-to-G mutation at the m^6A modification site in the endogenous FADS1 exon 10. lactate dehydrogenase (LDH) release assay and CCK-8 assay demonstrated that, compared to wild-type cells, the endogenous mutation at the m^6A modification site on the FADS1 exon 10 led to reduced sensitivity to RSL3-induced ferroptosis and decreased cytotoxicity. However, PSMD14 knockdown in the mutant cells did not result in notable decrease in RSL3-induced ferroptosis. In contrast, supplementation with exogenous AA in the mutant cells increased their sensitivity to RSL3-induced ferroptosis and enhanced cytotoxicity. The combination of PSMD14 knockdown and exogenous AA supplementation in the mutant cells did not exhibit notable increase in RSL3-induced ferroptosis compared to exogenous AA supplementation alone (fig. S6, M to P). In summary, when the specific m^6A modification site on FADS1 exon 10 is removed, the synthetic lethality induced by targeting PSMD14 plus exogenous AA supplementation in TNBC ceases to exist.

Meanwhile, another inducer of ferroptosis, Imidazole Ketone Erastin (IKE), has also been used to detect the effect of PSMD14 on susceptibility to ferroptosis, which is consistent with the results of RSL-3 treatment. PSMD14 deficiency is highly resistant to IKE-induced ferroptosis by suppressing lipid peroxidation, and, compared with the control group, additional AA combined with PSMD14 knockdown distinctly promoted the sensitivity to IKE (fig. S6, Q to T).

Whether ferroptosis depends on splicing of FADS1 mRNA regulated by m^6A was also further investigated. The role of FADS1 mRNA splicing in ferroptosis by using exogenous m^6A modification site mutations is to regulate the key role of FADS1 mRNA splicing and to examine the cell viability, LDH release, lipid peroxidation level, and ROS production. The results showed that m^6A modification site mutations promote FADS1 mRNA splicing, which reduced cell viability (fig. S7, A and B) and the release of LDH (fig. S7, C and D), as well as the levels of ROS (fig. S7, E and F) and lipid peroxidation (fig. S7, G and H), leading to decreased sensitivity to ferroptosis. In addition, as the LC-MS assay showed, compared with the control group, the levels of phosphatidylethanolamine, phosphatidylcholine, and part of high degree of unsaturation fatty acids were clearly decreased in the sh-PSMD14 group (fig. S7I). Collectively, all these data suggested that PSMD14 silencing are resistant to RSL3/IKE-induced ferroptosis via FADS1, which was rescued by exogenous AA supplementation in TNBC cells.

PSMD14 promotes TNBC progression via Akt/mTOR pathway and synthetic lethality with AA supplementation in xenograft models

To further confirm the biological effects of PSMD14 in vivo, we established a subcutaneous xenograft tumor model in BALB/c nude

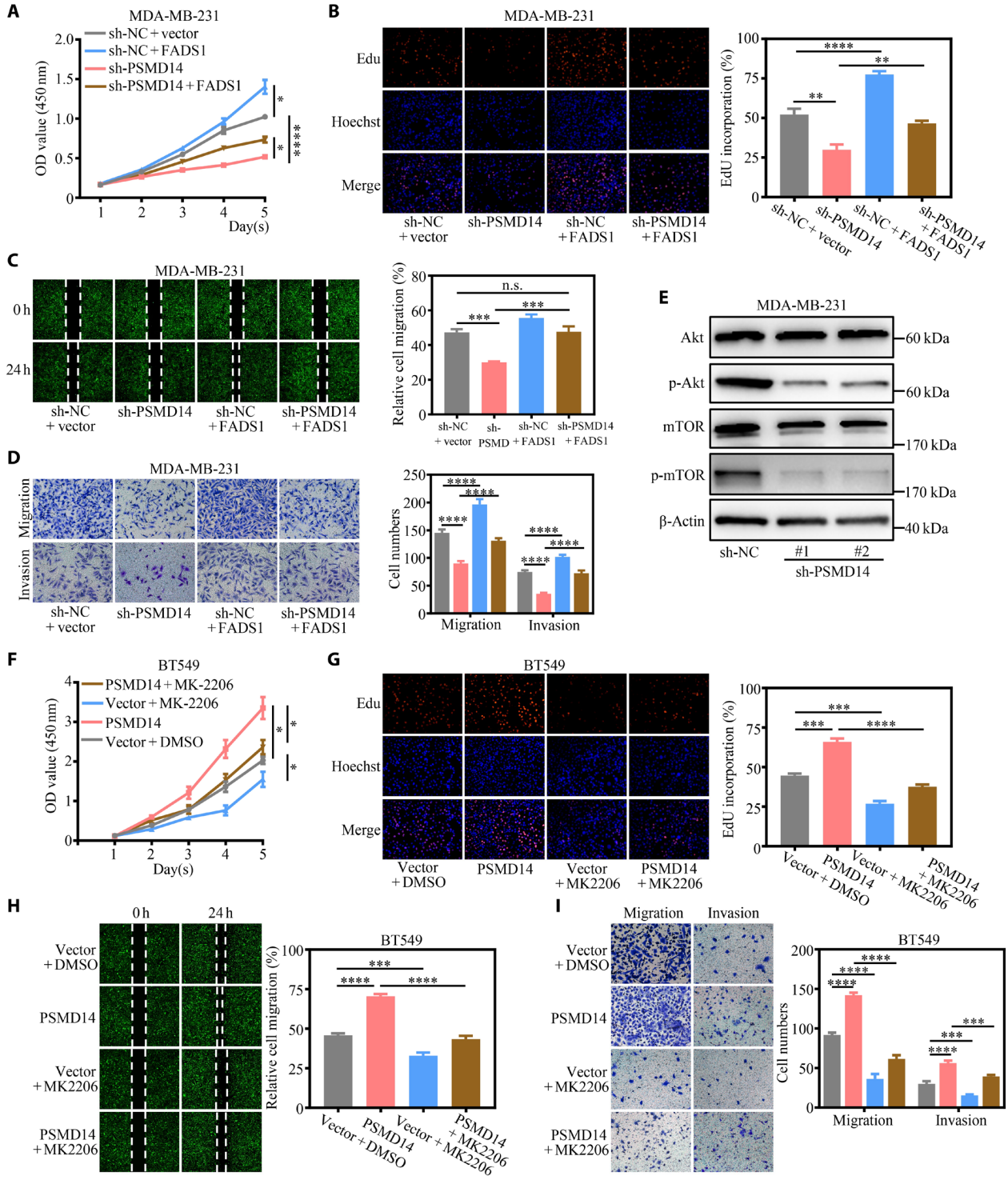

Fig. 6. PSMD14 promotes cell proliferation, migration, and invasion of TNBC through targeting FADS1/Akt/mTOR axis. (**A**) Cell proliferation assays for PSMD14-knockdown MDA-MB-231 cells with transiently transfected with FADS1 or the control. (**B**) Edu assays for PSMD14-knockdown MDA-MB-231 cells with transiently transfected with FADS1 or the control. (**C**) Wound-healing assay for PSMD14-knockdown MDA-MB-231 cells with transiently transfected with FADS1 or the control. (**D**) Representative images and cell count of migration and invasion assays for PSMD14-knockdown MDA-MB-231 cells with transiently transfected with FADS1 or the control. (**E**) Western blot analysis of protein expression of FADS1, Akt, p-Akt, mTOR, and p-mTOR upon PSMD14 knockdown in MDA-MB-231 cells. (**F**) Cell proliferation assay of TNBC cells overexpressing PSMD14 treated with Akt inhibitor (MK-2206) or control reagent. DMSO, dimethyl sulfoxide. (**G**) EdU assays of MDA-MB-231 cells overexpressing PSMD14 treated with Akt inhibitor (MK-2206) or control reagent. (**H**) Wound-healing assay of MDA-MB-231 cells overexpressing PSMD14 treated with Akt inhibitor (MK-2206) or control reagent. (**I**) Representative images and cell count of migration and invasion assays of MDA-MB-231 cells overexpressing PSMD14 treated with Akt inhibitor (MK-2206) or control reagent.

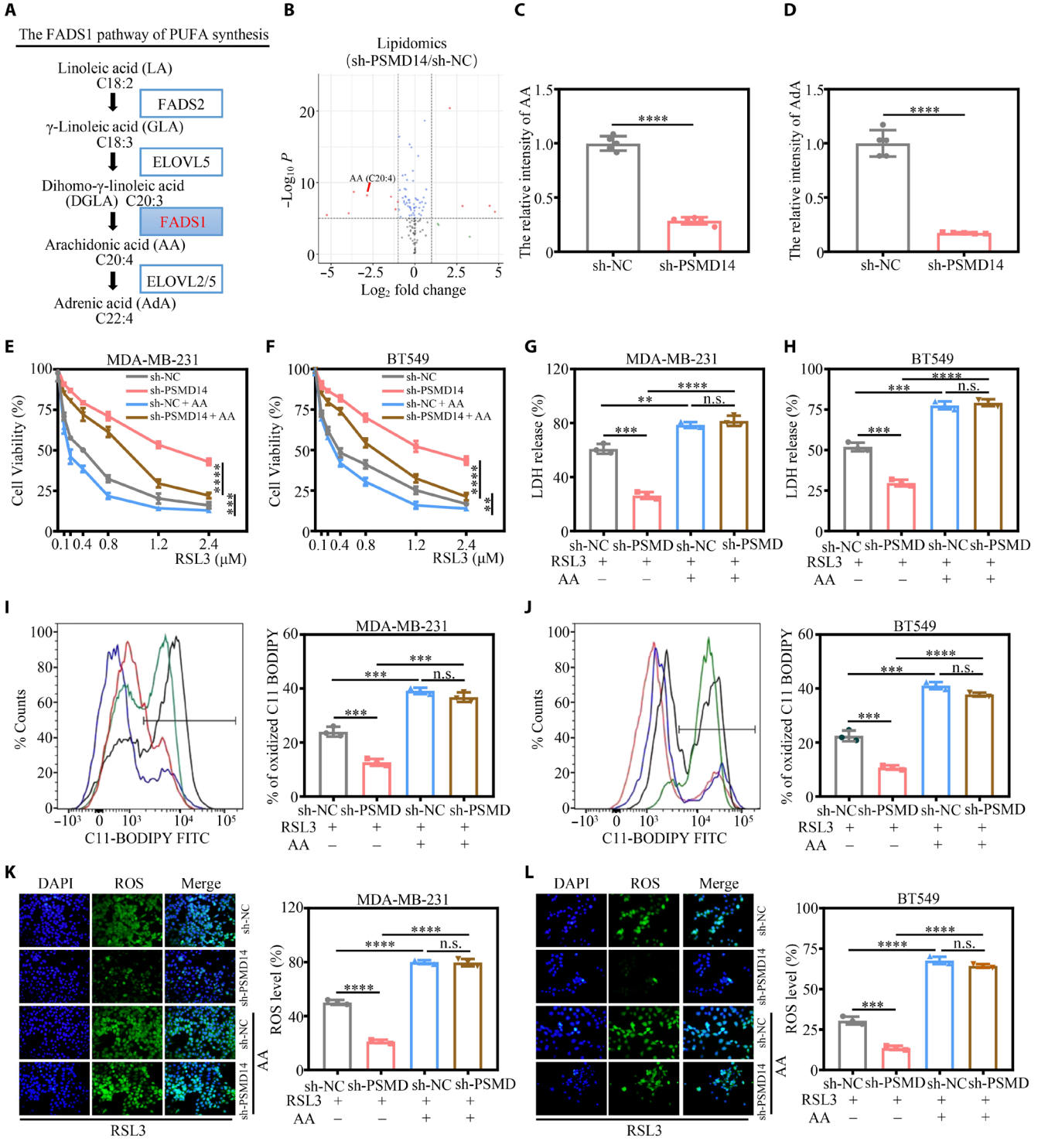

Fig. 7. Knockdown of PSMD14 combined with exogenous AA supplementation promoted the synthetic lethality of TNBC cells. (**A**) Scheme showing the fatty acids expression of FADS1 pathway. (**B**) Volcano plot showing fold changes and *P* values for lipid species in PSMD14 knockdown versus control (Ctrl) MDA-MB-231 cells. Free AA is highlighted. (**C** and **D**) Relative level of AA and AdA detected in PSMD14 knockdown versus Ctrl MDA-MB-231 cells using LC-MS/MS. (**E** and **F**) Relative cell viability in PSMD14-knockdown TNBC cells pretreated with 2.5 μM of AA for 24 hours and treated with RSL3 for 24 hours. (**G** and **H**) Relative lactate dehydrogenase (LDH) assay in PSMD14-knockdown TNBC cells pretreated with 2.5 μM of AA for 24 hours and treated with RSL3 for 24 hours. (**I** and **J**) Lipid peroxidation levels in PSMD14-knockdown TNBC cells pretreated with 2.5 μM of AA for 24 hours and treated with RSL3 for 24 hours. FITC, fluorescein isothiocyanate. (**K** and **L**) Reactive oxygen species (ROS) production was detected by fluorescence microscope (left) and fluorescence quantitative analysis (right) in PSMD14-knockdown TNBC cells pretreated with 2.5 μM of AA for 24 hours and treated with RSL3 for 24 hours.

mice by implanting BT-549 cells containing a control sequence or PSMD14 sequence. The tumor growth and weight were notably increased with PSMD14 overexpression but were markedly decreased with MK-2206 treatment. These effects were reversed by co-treatment with MK-2206 and PSMD14 ectopic expression (Fig. 8, A to C). Moreover, IHC assays further revealed that the enrichment of FADS1, Ki-67, SF3B4, p-Akt, and p-mTOR in xenograft tumors was increased by PSMD14 overexpression, but was distinctly attenuated by MK-2206 treatment. The protein expression levels of Ki-67, p-Akt, and p-mTOR were reversed by PSMD14 overexpression combined with MK-2206 treatment. Coincidentally, there were no notable differences in HNRNPC levels following treatment with MK-2206 or PSMD14 ectopic expression (Fig. 8, D and E).

Consistent with these findings, the volume, weight, and histochemical staining of the xenograft tumors were distinctly reduced after PSMD14 attenuation. Moreover, PSMD14 knockdown plus AA and RSL3 accelerated this reduction, whereas the ferroptosis inhibitor liproxstatin-1 reversed this effect (Fig. 8, F to H). Meanwhile, we also used IKE, an inducer of ferroptosis, to further confirm PSMD14-mediated sensitivity to ferroptosis in vivo. The results also indicated that the PSMD14 knockdown plus IKE and AA further inhibits tumor growth compared to PSMD14 knockdown or PSMD14 knockdown plus IKE (fig. S8, A to C). IHC staining showed that the protein expression levels of FADS1, Ki-67, SF3B4, p-Akt, and p-mTOR were decreased in xenograft tumors induced by PSMD14 knockdown in MDA-MB-231 cells, while the AA supplementation further lowered the level of Ki-67. Furthermore, the marker of ferroptosis, PTGS2, showed increased expression in the groups treated with RSL3 or IKE, and liproxstatin-1 was able to reverse this increased effect. Meanwhile, the AA supplementation also up-regulated the expression of PTGS2 when PSMD14 knockdown plus IKE (Fig. 8, I and J, fig. S8, D to E). As expected, PSMD14 down-regulation or AA with RSL3 treatment had no effect on the expression level of HNRNPC (Fig. 8, I and J, and fig. S8, D to E). In summary, these data showed that PSMD14 silencing strongly inhibited TNBC progression via the Akt/mTOR pathway in vivo, which synergistically exerted antitumor effects with exogenous AA supplementation.

OPA plus AA supplementation induced synthetic lethality in PSMD14-positive TNBC PDX and PDO models

As previously reported, inhibition of PSMD14/Akt/mTOR signaling inhibits TNBC proliferation, and exogenous AA supplementation reverses resistant to RSL3-induced ferroptosis due to PSMD14 deficiency. Therefore, we further explored the inhibition of PSMD14 combined with exogenous AA supplementation to induce synthetic lethality in TNBC. To better emulate the physical tumor microenvironment, we stablished preclinical TNBC models, PDX, and PDO models and treated them with OPA (a small-molecule inhibitor of PSMD14) (*6*), AA/RSL3, or combination therapy, to further verify the synthetic lethality induced by PSMD14 inhibition plus AA supplementation in PSMD14-positive TNBC (Fig. 9A). Consistent with our assumption, the tumor weights and volumes were substantial attenuated after treatment with OPA compared with the control group, whereas OPA combined with exogenous supplemental AA more notably inhibited tumor growth, exerting a synergistic effect (Fig. 9, B to D, and fig. S9, A to C). The IHC analysis revealed decreased Ki-67, p-Akt, and p-mTOR after treatment of OPA tumors. The combination treatment group exhibited the lowest levels of Ki-67, p-Akt, and p-mTOR, compared to treatment with AA and RSL3 alone (Fig. 9, E and F, and fig. S9, D and E). Additionally, microscopy was used to evaluate changes in the cells of three PDO models after single treatment and combination treatment. Result showed that cells lost their normal shape and became shrunken in the OPA-treated group, whereas the condensations and cristae were more obvious in the combination treatment group (Fig. 9G). Similarly, the combination therapy led to the most substantial reduction in tumor organoid cell viability (Fig. 9G). Moreover, Ki-67 immunostaining of PDOs showed a marked decrease in the OPA plus AA/RSL3 group (Fig. 9, I and J). These results showed that, upon exogenous AA and RSL3 supplementation, ferroptosis in the cell model was consistent with our expectations.

DISCUSSION

In this study, we found that PSMD14 was up-regulated in TNBC tissue samples and its high expression was positively correlated with a poor prognosis. Moreover, PSMD14 played a carcinogenic role by deubiquitinating SF3B4, promoting protein stabilization of SF3B4 and then mediating alternative splicing regulation of HNRNPC/SF3B4 complex through m^6A modification pathway. The HNRNPC recognized m^6A-modified FADS1 and PSMD14 overexpression promoted exon inclusion of FADS1, while PSMD14 silencing facilitated exon skipping. Meanwhile, we further aimed to explore the underlying functional mechanism of FADS1 and revealed that PSMD14 aggravated TNBC malignant progression by activating the Akt-mTOR signal pathway mediated by FADS1. In addition, PSMD14 silencing was resistant to ferroptosis induced by RSL3/IKE. However, exogenous AA supplementation reverses resistant to RSL3/IKE-induced ferroptosis due to PSMD14 deficiency, PSMD14 silencing combined with exogenous AA supplementation induce synthetic lethality in TNBC (Fig. 9K).

The results of previous studies have indicated that PSMD14 can regulate the attachment residues of K11, K48, and K63 ubiquitin in cancer (*10*, *11*, *31*), leading to different fates of substrate proteins. The decrease K48-linked ubiquitination on GRB2 induced by PSMD14 increases the stability of GRB2, leading to an increase in GRB2 protein levels and promoting the progression of hepatocellular carcinoma (*31*). The deubiquitylation of K11- and K63-linked polyubiquitin chains on transcription factor E2F1 mediated by PSMD14 contributes to its stability and carcinogenicity (*10*). PSMD14 can inhibit lysosomal degradation and increase transforming growth factor–β by removing K63 polyubiquitin chains attached to caveolin-1, which participates in lysosome-dependent destruction of receptors (*11*). However, the specificity of K63 polyubiquitin chains was considered a characteristic of the JAMM family of DUB (*32*). Consistent with this work, we observed that PSMD14 only reduced the polyubiquitin chain connected to K63 on SF3B4 in TNBC cells, altering the form of SF3B4 oligomers to regulate the stability of SF3B4 protein. Herein, we found that PSMD14 promotes the progression of TNBC by regulating FADS1 through the m^6A modification pathway mediated by the HNRNPC and SF3B4 complex, which is achieved by deubiquitylation of SF3B4.

HNRNPs, a family of multifunctional protein molecules, are the m^6A reader proteins that were identified to play a crucial role in the m^6A recognition process by selectively identifying m^6A-modified mRNA sites (*33*). Previous studies showed that HNRNPC was involved in a variety of processes, including AS, stability of mRNAs, and translation regulation (*34*–*36*), and is highly expressed in various cancers (*37*, *38*). Recent studies have shown that m^6A modifications

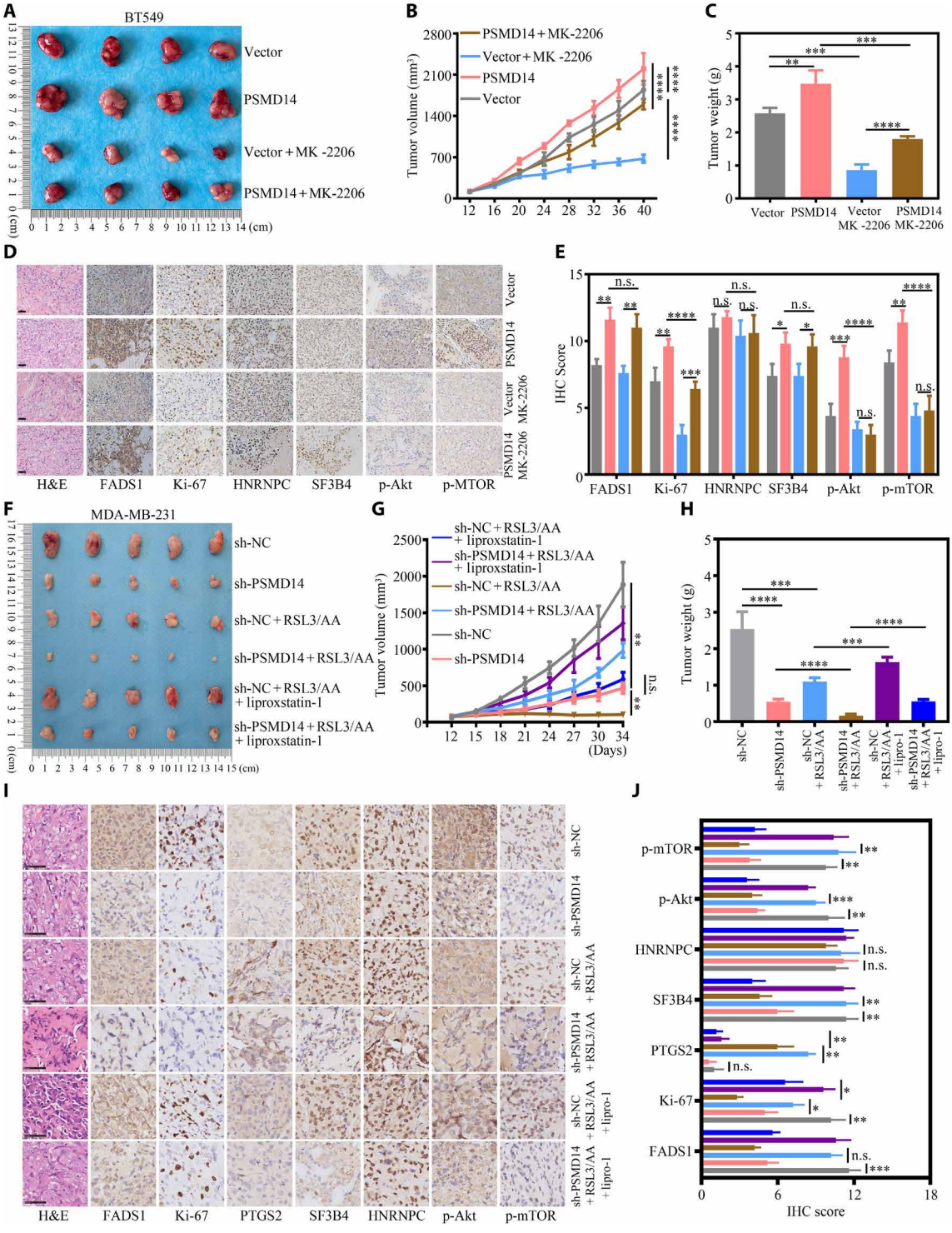

Fig. 8. PSMD14 drives TNBC tumorigenesis and mediates sensitivity to ferroptosis in vivo. (**A**) Response of expressing vector or PSMD14 xenografts to treatment with PBS or MK-2206. The representative images of xenograft tumor in each group were displayed ($n = 4$). (**B**) The tumor volumes were measured twice a week and the growth curves were drawn. (**C**) Tumor weight of was analyzed. (**D** and **E**) Representative images and quantification of hematoxylin and eosin (H&E) and immunostaining (scale bars, 50 μm) of FADS1, Ki-67, HNRNPC, SF3B4, p-Akt, and p-mTOR in tumors of nude mice. (**F**) Response of expressing vector or sh-PSMD14 xenografts to treatment with PBS, RSL3/AA, or liproxstatin-1; the representative images of xenograft tumor in each group were displayed ($n = 5$). (**G**) The tumor volumes were measured twice a week, and the growth curves were drawn. (**H**) Tumor weight of was analyzed. (**I** and **J**) Representative images and quantification of H&E and immunostaining (scale bars, 50 μm) of FADS1, Ki-67, PTGS2, HNRNPC, SF3B4, p-Akt, and p-mTOR in tumors of nude mice. lipro-1, liproxstatin-1.

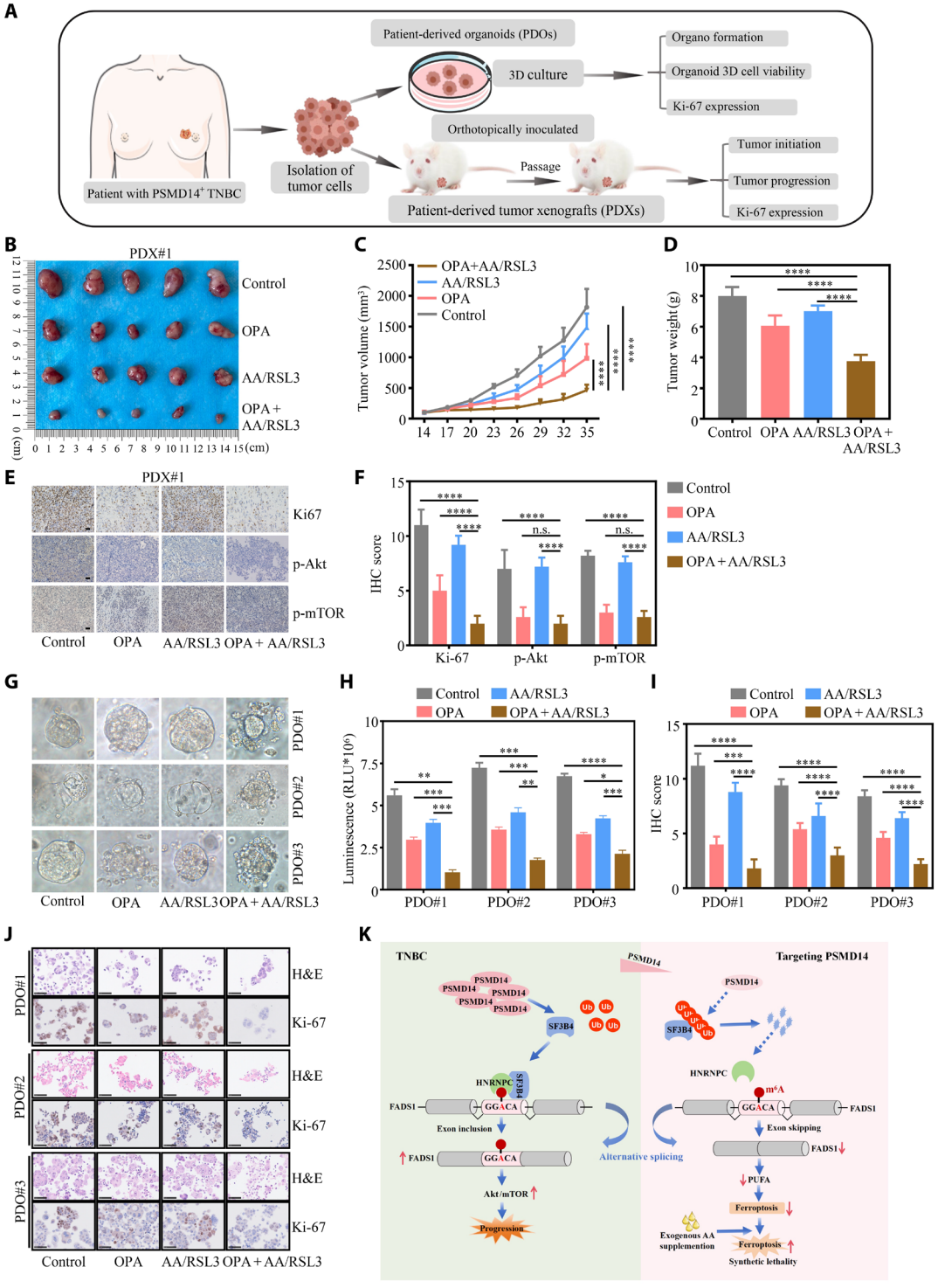

Fig. 9. OPA plus AA supplementation induced synthetic lethality in PSMD14-positive TNBC PDXs and PDOs. (**A**) Graphic illustration of PSMD14^{+} TNBC PDX and PDO mouse models. (**B**) The xenograft tumors of PDX mice treated with OPA, AA/RSL3, OPA combined with AA/RSL3, and vehicle control were collected. (**C**) Tumor volume was monitored in PDX mice every 3 days, and tumor growth curves were generated. (**D**) The tumors in PDX mice were extracted and weighed. (**E**) Sections of tumors in PDX mice were stained with anti–Ki-67, anti–p-Akt, and anti–p-mTOR antibodies by IHC (scale bars, 100 μm). (**F**) Quantification of Ki-67–, p-Akt–, and p-mTOR–positive staining in PDX tumors. (**G**) Bright-field images depicting the major phenotypes of TNBC organoids treated with OPA, AA/RSL3, OPA combined with AA/RSL3, and vehicle control, respectively. (**H**) Viability of organoids detected by CellTiter-Glo 3D cell viability assay after the indicated treatments as described in (G). (**I**) Quantification of Ki-67–positive staining in organoids. (**J**) Histological and IHC images showing the organization structure and status of proliferation marker (Ki-67) in organoids after the indicated treatments as described in (G) (scale bars, 50 μm). (**K**) A graphical representation of PSMD14 promoting the exon inclusion of FADS1 via the m^{6}A modification, activating the FADS1/Akt/mTOR signaling pathway to promote TNBC progression, and targeting PSMD14 in combination with exogenous AA–inducing synthetic lethality in TNBC by increasing sensitivity to ferroptosis. RLU, relative light unit.

can regulate alternative splicing patterns by recruiting specific RNA binding proteins (RBPs) that regulate alternative splicing and influencing the interaction between RBP and its target RNAs (*16*). Additionally, studies have shown that m^6A reader can regulate mRNA splicing and promote exon inclusion (*28*). On the basis of this, we speculated that HNRNPC, which is the m^6A reader protein, is also involved in the regulation of alternative splicing in TNBC. In our study, we performed RNA-pulldown assay, mass spectrometry analysis, RIP assay, and MeRIP assay to verify that HNRNPC acted as an RBP protein, as well as an m^6A reader, to recognize and bind to m^6A-modified FADS1 and promote exon inclusion of FADS1.

Studies have shown that m^6A reader can act as a recruiter for mRNA splicing factors during alternative splicing, which requires the combination with appropriate splicing factors to exert regulatory effects on alternative splicing (*28*). SF3B family members act by binding with the U2 small nuclear ribonucleoprotein and regulating the AS of pre-mRNA (*39*), and they have been shown to affect the progression of various cancers (*40*–*42*). SF3B4, a vital subunit of SF3B, was involved in the process of transcription, translation, cell signaling regulation, and pre-mRNA splicing (*43*). However, the potential mechanism of SF3B4 in the development of TNBC remains to be elucidated. In this study, the RBP SF3B4 acts as an mRNA splicing factor, consistent with PSMD14 to promote exon inclusion of FADS1. However, exon skipping was enhanced in the absence of PSMD14, which led to down-regulation of FADS1.

Studies have shown that FADS1 is a biomarker for survival in patients with cancer, plays various roles in the biology of cancer, and represents a potential target for precision therapy in cancer (*44*). Meanwhile, FADS1 can promote the progression of laryngeal squamous cell carcinoma by activating the Akt/mTOR signaling (*29*). In this study, we found that FADS1 can act as a functional downstream target of PSMD14, and PSMD14 can promote the progression of TNBC through the FADS1/Akt/mTOR signaling pathway. This elucidated a mechanism for malignant progression of TNBC and provided a perspective for potential therapeutic targets, including the PSMD14/FADS1/Akt/mTOR regulatory axis.

In addition, FADS1 has been identified as the key rate-limiting enzyme in the process of bioactive metabolites, converting DGLA to AA (*24*). FADS1 is up-regulated in colorectal cancer and effectively mediates the synthesis of AA, thus promoting colorectal cancer tumor growth via high-AA microenvironment-induced enriched gram-negative microbes (*45*). Previous studies have shown that AA (20:4), an omega-6 PUFA that is an essential component for ferroptosis, enhances RSL3-induced ferroptosis in mouse embryonic fibroblasts in vitro (*46*). In this study, we found that, compared to normal tissue, tumor tissue has higher expression of FADS1 and higher concentrations of AA. Studies have shown that deficiency of FADS1 resulted in cancer cell resistance to ferroptosis, and sensitivity was restored with exogenous AA supplementation, as determined by the PUFA synthesis pathway that plays an important role in ferroptosis (*23*). It is noteworthy that, in this study, PSMD14 knockdown notably reduced the expression of AA and decreased the sensitivity of cells to RSL3/IKE-induced ferroptosis. Exogenous AA supplementation could restore the sensitivity of cells to RSL3/IKE-induced ferroptosis. Therefore, the targeting PSMD14 combined with the supplementation of exogenous AA will induce the synthetic lethality of TNBC cells. This is because, while targeting PSMD14 can block the FADS1/Akt/mTOR signaling pathway to inhibit the growth of TNBC cells, at this point, there is no notable necrosis of cancer cells, which may be due to the decreased sensitivity to ferroptosis upon PSMD14 deficiency. Therefore, exogenous AA supplementation reverses this reduced sensitivity and, combined with PSMD14 deficiency, induced the synthetic lethality in TNBC.

In conclusion, our study was devoted to improving our understanding of PSMD14 in tumor progression and elucidating the molecular mechanisms and providing a potential therapeutic strategy for future treatment. Perhaps in the future, for patients with high PSMD14 expression, ferroptosis therapy in combination with PSMD14 inhibitor treatments can achieve better therapeutic results.

MATERIALS AND METHODS

TNBC tissue specimens, cell lines, and cell culture

TNBC tissues and adjacent normal tissues were obtained from 65 patients admitted at the Union Hospital of Tongji Medical College from January 2018 to May 2021. The postoperative histopathological diagnosis of all patients was invasive ductal TNBC. The cell lines MCF10A and MDA-MB-468 were from Guangzhou Cellcook Biotech, and MDA-MB-231, MDA-MB-157, BT549, BT20, Hs578T, and HCC1937 came from the American Type Culture Collection. These cell lines were cultured in recommended medium at 37°C humidity with 5% CO_2 and were validated to be free of *Mycoplasma*. These cells were subjected to short tandem repeat analysis.

Plasmid, lentivirus production, and cell transduction

Knockdown plasmids sh-PSMD14, sh-HNRNPC, and sh-SF3B4; overexpression plasmid OE-PSMD14; overexpression plasmid OE-FADS1; and the control (empty vector) were obtained from GenePharma (China). In brief, pLKO.1 puro-sh-PSMD14 #1, puro-sh-PSMD14 #2, puro-sh-PSMD14 #3, puro-sh-HNRNPC, puro-sh-SF3B4, and control vectors were transfected into human embryonic kidney 293T cells. After 48 hours of transfection, supernatants containing lentivirus particles were collected and filtered. TNBC cells were incubated with the supernatants for 24 hours, and puromycin was used to screen stably transfected cell lines. The oligo sequences of sh-PSMD14 #1, sh-PSMD14 #2, and sh-PSMD14 #3, sh-HNRNPC, sh-SF3B4, and sh-FADS1 were synthesized by GenePharma (China), and these are listed in table S1.

Cell proliferation assays

Cell proliferation was assessed by using CCK-8 assay, EdU assay, and colony formation assay according to the manufacturer's protocol. For CCK-8 assay, cells (5×10^3 cells per well) were seeded into 96-well plates. After 10 μl of CCK-8 solution (Dojindo, Japan) was added at the indicated time points and incubated at 37°C for 1 to 3 hours, the absorbance was measured at 450 nm on a microplate reader (Thermo Fisher Scientific, USA). For EdU assays, cells (2×10^4 cells per well) were seeded into 96-well plates and incubated with 100 μl of medium containing 50 mM EdU (Beyotime, China) for 2 hours. Then, the cells were fixed with paraformaldehyde and stained with Apollo dye solution, while the nuclei were stained with Hoechst. Images were captured using a fluorescence microscope (Nikon). For colony formation assays, cells (1×10^3 cells per well) were seeded into six-well plates cells and cultured in complete medium at 37°C for 2 weeks. After the medium was removed, the colonies were washed with phosphate-buffered saline (PBS), fixed with paraformaldehyde (Thermo Fisher Scientific, USA) for 10 min, and then visualized using crystal violet (Beyotime, China) staining for 20 min. The colonies were counted and imaged.

Transwell and wound-healing assays

For the cell migration and invasion transwell assays, the 24-well Transwell chamber system (Corning, USA) was used. Cells (3×10^4) in 200 μl of serum-free medium were seeded into the top chambers of transwell inserts, while 700 μl of culture medium with 20% FBS was added to the lower chamber. The upper 24-well Transwells were coated with Matrigel (Sigma-Aldrich, USA) before plating cells during invasion assays. The cells were stained with crystal violet, imaged, and counted under a microscope (×20). For wound-healing assay, cells (5×10^5) were cultured in six-well plates, with 2 ml for each well. Once the cells were overgrown, they were scratched in a straight line with a pipette tip, and exfoliated cells were removed. At the indicated time points, the distance of cell migration to the middle of the scratch was observed under a light microscope with green color, and the cells were imaged at ×40 magnifications.

Western blot and IHC assays

Western blotting and IHC assays were performed as previously reported (*47*). The following antibodies were used: PSMD14 (1:1000; 12059-1-AP, Proteintech), HNRNPC (1:1000; 11760-1-AP, Proteintech), SF3B4 [1:1000; 80026S, Cell Signaling Technology (CST)], FADS1 (1:500; 10627-1-AP, Proteintech), Akt (1:1000; A20799, ABclonal), p-Akt (1:1000; 66444-1-Ig, Proteintech), mTOR (1:1000; 66888-1-Ig, Proteintech), p-mTOR (1:1000; 67778-1-Ig, Proteintech), β-actin (1:1000; 8457S, CST), Ki-67 (1:200; 27309-1-AP, Proteintech), PTGS2 (1:200; 66351-1-Ig, Proteintech), and DYKDDDDK Tag (1:1000; no. 14793, CST).

RNA extraction and RT-qPCR

Total RNA was extracted from tissues and cells by using RNAiso Reagent (Takara, Dalian, China) according to the user's manual. Reverse transcription was performed using a PrimeScript RT kit (Takara, China), and PCR analysis was performed using TB Green premix Ex-Taq (Takara, China). The mRNA relative expression levels were quantitated using the $2^{-\Delta\Delta Ct}$ method and normalized by glyceraldehyde-3-phosphate dehydrogenase 1. The sequences of primers used in this study are listed in table S2.

Immunofluorescence

Cells were seeded into confocal dish and fixed in 4% paraformaldehyde (Thermal Sciences, USA) for 30 min and then washed three times with PBS (Sigma-Aldrich, USA, 5 min per wash). Next, the cells were permeabilized with 0.5% Triton X-100 in PBS for 15 min at room temperature and then washed three times with PBS (5 min per wash). After permeabilization, the cells were incubated with specific antibody overnight at 37°C. Nuclei were stained with 4′,6-diamidino-2-phenylindole. The staining results were observed using a confocal fluorescence microscope.

Co-immunoprecipitation

The Co-IP assay was conducted by using the Co-Immunoprecipitation Kit (Beyotime Biotechnology, P2197M) according to the manufacturer's protocol. Cells were lysed by buffer [20 mM tris-HCl (pH 7.6), 100 mM NaCl, 20 mM KCl, 1.5 mM $MgCl_2$, and 0.5% NP-40] containing Protease Inhibitor Cocktail (Selleckchem, USA). Cell lysate was incubated with anti-PSMD14, anti-HNRNPC, or anti-SF3B4 antibody overnight and followed by incubation with protein A/G agarose for 4 hours. Then, denatured immunoprecipitated samples were added to SDS–polyacrylamide gel electrophoresis (PAGE) gels and transferred onto polyvinylidene difluoride membranes, followed by immunoblotting with the corresponding antibodies.

In vivo ubiquitination assay

In vivo ubiquitination assays were performed according to the protocols described. Lysates were incubated at 4°C for 15 hours with the indicated antibodies and protein G agarose beads. The beads were washed four times with lysis buffer, and samples were boiled for 5 min with 2× sample buffer. Immunoprecipitation samples were transferred onto nitrocellulose (NC) membranes, and the membranes were denaturated by 6 M guanidine hydrochloride buffer [20 mM tris-HCl (pH 7.5) buffer containing 6 M guanidium chloride and 5 mM β-mercaptoethanol] at 4°C for 30 min. Subsequently, membranes were washed with washing buffer three times. After the denaturation and washing steps, membranes were blocked in 5% bovine serum albumin for 2 hours and incubated with anti-SF3B4 antibody (BML-PW9910; Enzo Life Sciences, Farmingdale, USA) at 4°C overnight. Each ubiquitination was examined by an immunoblotting assay.

Immunoaffinity purification of HA-PSMD14–associated proteins

Cells were transfected with either the control vector or HA-PSMD14. Two days after transfection, the cells were harvested and washed with PBS twice. The cells were lysed with EBC buffer [20 mM tris-HCl (pH 8.0),125 mM NaCl, 2 mM EDTA, and 0.5% NP-40] with the addition of protease inhibitors. After removing cell debris by high-speed centrifugation, cell lysates were precleared with protein A–conjugated Sepharose beads for 2 hours at 4°C with gentle agitation. Then, the anti-FLAG M2 agarose beads were added and incubated for 3 hours at 4°C with rotation. Beads were washed five times with EBC buffer for 10 min each. SDS loading buffer was added directly to the beads and boiled for 5 min before samples were loaded and separated by 8% SDS-PAGE.

RNA-seq and DEG analysis

Total RNA was extracted from MDA-MB-231 cells treated with shRNA against either sh-PSMD14 or sh-NC. Using a TruSeq Stranded Total RNA kit with Ribo-Zero H/M/R treatment (Illumina) and sequenced on an Illumina Novaseq6000 Sequencing system to produce the RNA library. DEGs analysis between two groups were performed. A heatmap clustered was used to show DEGs. Last, DEGs between two groups were obtained by paired *t* test with $P < 0.05$.

Analyses of differential splicing genes

To screen DSGs in breast cancer tissues and adjacent normal tissues, the differential AS events from RNA-seq data were examined by rMATS. A false discovery rate < 0.05 was considered to be the threshold for judging the significance of the DSGs.

RNA binding protein immunoprecipitation

All the specific manipulations were performed according to the protocol of Magna RIP RNA-Binding Protein Immunoprecipitation Kit (Merck Millipore, 17–700). Antibodies used for the RIP assay included anti-SF3B4, anti-HNRNPC, and immunoglobulin G. RNAs were extracted with RNAiso Reagent and subjected to qPCR analysis. The primers for RT-qPCR are listed in table S2.

Methylated RNA immunoprecipitation

All the specific manipulations for MeRIP assays were performed according to the protocol of the Magna MeRIP m^6A Kit (Merck

Millipore, 17–10499). The eluted RNA was purified with an RNeasy MiniElute Cleanup kit (QIAGEN, 74204) and then subjected to qPCR with One Step TB Green PrimeScript RT-PCR Kit (Takara, RR066A). The primers for RT-qPCR are listed in table S2.

RNA-pulldown assay

Biotin-labeled RNAs were synthesized by Tsingke. RNA probes included probes that contained an m^6A base, or an adenine base mutation, or a guanine base mutation. The RNA-pulldown assay was performed by using the Pierce Magnetic RNA-Protein Pull-Down Kit (Thermo Fisher Scientific, 20164). The eluted protein samples were denatured with SDS buffer and detected by Western blotting with the corresponding antibodies.

Lipid analysis using LC-MS/MS

For whole lipid mass spectrometry, 1×10^7 cells were washed twice with prechilled PBS. The cells on the culture dish were scraped into 1 ml of prechilled methanol:water (4:1) to extract the cellular lipids. After centrifugation at low temperature, the supernatant was transferred to a new Eppendorf (EP) tube, and 2 ml of chloroform and 1 ml of 0.1 M HCl were added. The mixture was removed by centrifugation. Lipid extracts were dried under nitrogen and reconstituted with 250 μl of isopropanol:acetonitrile:water (2:1:1) solution. Lipid analysis was performed using an ACQUITY UPLC system (Waters, Milford, MA, USA). Chromatographic separation was performed at 35°C using an Acquity UPLC BEH C18 column (2.1 mm by 100 mm, 1.7 μm; Waters). To determine peaks, perform comparisons, and generate peak tables of mass/charge ratio values and sample retention times, spectral data were analyzed using a MarkerView 16 (AB Sciex).

Cell viability and LDH release assays

Using a CellTiter-Glo reagent (CellTiter-Glo 2.0 Assay, G9243, Promega) kit, cell viability was determined according to the manufacturer's instructions. The LDH release assay was performed using a cytotoxicity detection kit (11644793001, Roche).

Lipid peroxidation assay

The lipid peroxidation was measured by C11 BODIPY 581/591 flow cytometry. First, on the day before the experiment, 2×10^5 cells were inoculated into each well of a six-well plate. To measure lipid peroxidation levels, the cells were treated with RSL3 (1 μM) and then incubated with 2.5 μM C11 BODIPY 581/591 for 15 min. The cells were then collected by trypsin digestion, transferred to a 1.5-ml microcentrifuge tube, pelleted (3000 rpm, 3 min), and then suspended in 0.5 ml of PBS. A 488-nm laser flow cytometer (BD-FACSCalibur) was used for excitation analysis of cells, and data were collected from an FL1 detector. FlowJo software was used to analyze data.

Construction of mutant exogenous plasmid containing FADS1 exon 10 m^6A modification site

The mutant plasmid pCDNA3.1-FADS1(human)-Mut-3×FLAG, with $A(m^6)$ mutation to G in $GGA(m^6)CA$ on exon 10, was derived from pGFP–epidermal growth factor receptor through site mutagenesis performed by Wuhan Tsingke Biotech Co. Ltd. Briefly, using FADS1(human)-WT in pCDNA3.1(+)-3×Flag plasmid as the template, PCR amplification was performed to obtain full-length sequence of FADS1(human)-Mut in pCDNA3.1(+)-3×Flag. For primer design: forward, 5′-CTTCAATGACTGGTTCAGTGGACACCTCAACTTCCAGATTG-3′; and reverse, 5′-CAATCTGGAAGTTGAGGTGTCCACTGAACCAGTCATTGAAG-3′. The recombinant plasmid was designated Mut-m^6A-Exo.

Design and construction of sgRNA containing CRISPR-Cas9 plasmids

Human FADS1 genomic sequence was obtained from the Ensemble database, and the sequences of exons 1 and 2 from the FADS1 (gene ID: 3992) were loaded onto the CRISPOR online-tool (http://crispor.tefor.net/crispor.py). Through the evaluation of the specificity and predicted off-target mismatches, we designed and selected three candidate single-guide RNAs (sgRNAs) for each exon. The target sequences used for genome editing were as follows: sgRNA#1, AGTTCATATACTTCTTCACA; sgRNA#2, CAGGGTCTTACATTCTTGGT; and sgRNA#3, TTGATGTGGAAGGCCACAAA. sgRNA under control of the human U6 promoter was synthesized and cloned into LentiCRISPRv2 puro vector. Pooled cells were selected using puromycin (10 μg/ml) and were confirmed by Western blotting. Last, the plasmid FADS1 sgRNA#1 was prepared for the virus packaging.

CRISPR-Cas9 knock-in of endogenous mutation at the FADS1 exon 10 m^6A modification site in MDA-MB-231 cells

To introduce point mutation into FADS1 exon 10 m^6A modification site, the RNP complex was used. Briefly, Cas9 protein and sgRNA were incubated at room temperature for 10 to 20 min, mixed with single-stranded oligonucleotides, followed by electrotransfection in a total of 1×10^7 MDA-MB-231 cells according to the manufacturer's instructions. After 48 hours of electrotransfection, cells were diluted by limited dilution method and inoculated into a 96-well plate. Selection of individual clones was screened 10 days later, and the mutated clones were validated by PCR and Sanger sequencing. The sgRNA was designed by using the online CRISPR design tool (Red Cotton, Guangzhou, China; https://en.rc-crispr.com/) and the hFADS1-gRNA sequence: GCCTTCAATGACTGGTTCAGTGG. The primer sequence of Oligo 1 [hFADS1-c.A1302G(GGA>GGG, p.G434G)] was 5′-accctgcttccccaggctccctactcacTGGTGCTCAATCTGGAAGTTGAGGTGCCCAGAGAACCAGTCATTGAAGGCAGACTTGTGGACATTGCATGTGGCCTGGAGctggcggaaaagg-3′. The mutation was designated m^6A-MT-En.

NB analysis

NB analysis of the FADS1 of different mRNA sizes was performed by following the instructions of the DIG Northern Starter Kit (Roche). First, FADS1-specific DNA template containing T7 promoter sequences from RT-PCR was purified by phenol-chloroform extraction and ethanol precipitation. Then, the digoxigenin (DIG)–labeled RNA probes were produced by using DIG RNA labeling Mix (Roche) with the DNA template. Then, DIG-labeled probes were used for hybridization to Hybond-N^+ membrane, and total RNA was determined by blotting on a positive capillary transfer system and was ultraviolet cross-linked. Last, the hybridized probes were detected with anti–DIG-AP and then were visualized with the chemiluminescence substrate CSPD. The signals were also captured by ChemiDoc XRS Molecular Imager system (Bio-Rad). The NB probe was CATCCCCTCCCAAAACTAAGTGGAGGCTCTGTCTTTTCCTCCTAGTTTGAGGTTCTCTTCTCCCAGTGTCTAAAATGATCAATATGCCTAGAGTAGATGCTGCTGAAGAGGCAAAGTAGTAATCCTGCCACCTGGAAGCAAAGGCTGTGGGTTGGAGGGGGAAGCGGGTGTGAGGGCTGATGA.

Tumor xenograft model

TNBC cells (1×10^7) infected with different lentiviruses were injected subcutaneously into 4-week-old female BALB/c nude mice. All procedures were performed in accordance with the National Institutes of Health *Guide for the Care and Use of Laboratory Animals* and were approved by the Animal Care and Use Committee of Tongji Medical College, Huazhong University of Science and Technology. When the tumor grew to 50 to 100 mm^3, the tumor-bearing mice with stable PSMD14 knockdown, and the controls were intraperitoneally injected liproxstatin-1 (10 mg/kg, once every day), RSL3 (100 mg/kg, twice a week), or IKE (50 mg/kg, once every other day). The tumor volume was calculated according to the formula: (length × $width^2$)/2. After 8 weeks, the mice were euthanized and tumors were excised and weighed. The collected tumor samples were preserved at −80°C.

TNBC PDX establishment

NSG mice were used to establish a TNBC PDX model. Animal experiments were approved by the Institutional Animal Care and Use Committee, Huazhong University of Science and Technology, and conducted in strict accordance with the Institutional Guidelines and Protocols. Fresh tumor tissues were collected from two patients with TNBC after surgical resection at the Wuhan Union Hospital and stored in iced Dulbecco's modified Eagle's medium (DMEM). Primary TNBC specimens were cut into 2- to 3-mm^3 pieces, mixed with an equal volume of Matrigel matrix (Corning, 354348), and then subcutaneously implanted into the flanks of NSG mice. When the tumors grew to ~50 to 100 mm^3 in size after injection of cancer cells, mice were randomly divided into four groups ($n = 5$ per group): an OPA treatment group that received intraperitoneal injection of OPA daily (5 mg/kg), a AA/RSL3 treatment group that received oral gavage of 10 mg of AA daily and was administered intratumorally injection of RSL3 (100 mg/kg, twice a week), an OPA plus AA/RSL3 group, and a control group that was intraperitoneally administered normal saline for 3 weeks. The diameter and width of tumors in PDX mice were measured every 3 days and tumor volume was calculated using the formula $V = 0.5 \times D \times W^2$ (V, volume; D, diameter; and W, width). All mice were executed at the appropriate time; the tumors were removed, photographed, and weighed; and further pathological analysis was done.

TNBC PDO culture

TNBC tissues were cut into small pieces and mechanically homogenized. The homogenized tissue was digested with trypsin on ice. After centrifugation, single-cell suspensions were added dropwise with cold 3D Matrigel matrix (Corning, 354348) to six-well culture plates, which were kept inverted in a cell incubator for 30 min before organoid-specific medium was added. Organoids were cultured with medium containing 1% GlutaMAX (Thermo Fisher Scientific, 35050061), Primocin (100 μg/ml; InvivoGen, 26-69-PM), hydrocortisone (0.5 μg/ml; MedChemExpress, HY-N0583), 10 μM Y27632 (Sigma-Aldrich, Y0503), 0.2 nM Wnt3a (StemRD, W3a-H-025), R-spondin1 (250 ng/ml; PeproTech, 120-38), Noggin (100 ng/ml; PeproTech, 120-10D), 1× B27 and vitamin A (Invitrogen, 17504-044), 10 mM Hepes (Thermo Fisher Scientific, 15630080), fibroblast growth factor–10 (20 ng/ml; Peprotech, 100-26), epidermal growth factor (5 ng/ml; Peprotech, GMP100-15), 10 mM nicotinamide (Selleckchem, S1899), 100 nM β-estradiol (Sigma-Aldrich, E2758), 10 μM forskolin (MedChemExpress, HY-15371), 5 nM heregulin B1 (ProSpec, CYT-733), 0.5 μM A83-01 (MedChemExpress, HY-10432), 0.5 μM SB202190 (Selleckchem, S10077), 1.25 mM *N*-acetylcysteine (Sigma-Aldrich, A0737), and DMEM.

Statistical analysis

All results were presented as the means ± SD. SPSS software was used for statistical analyses. Comparisons between two groups were performed with Student's *t* test. The expression of PSMD14 in 65 TNBC tissues and paired adjacent noncancerous tissues was analyzed using the paired *t* test. The relationships between the expression of PSMD14 and clinical characteristics of TNBC were analyzed by the chi-square test. P values < 0.05 were considered statistically significant. $^*P < 0.05$, $^{**}P < 0.01$, $^{***}P < 0.001$, and $^{****}P < 0.0001$.

Ethics statement

The human tumor tissues and paired adjacent normal tissues from patients at Wuhan Union Hospital, Huazhong University of Science and Technology, were collected after obtaining written consent from the patients. All experimental procedures involving patients were conducted in accordance with the ethical guidelines of the Declaration of Helsinki and were approved by the Institutional Human Ethics Committee of Tongji Medical College, Huazhong University of Science and Technology, Wuhan, China (S093). Furthermore, all the animal experimental procedures were performed in strict accordance with the guidelines of the Institutional Animal Care and Use Committee, Huazhong University of Science and Technology, Wuhan, China (S-3815).

Supplementary Materials

This PDF file includes:

Supplementary Text
Figs. S1 to S9
Tables S1 to S6

REFERENCES AND NOTES

1. R. L. Siegel, K. D. Miller, H. E. Fuchs, A. Jemal, Cancer statistics, 2022. *CA Cancer J. Clin.* **72**, 7–33 (2022).
2. W. D. Foulkes, I. E. Smith, J. S. Reis-Filho, Triple-negative breast cancer. *N. Engl. J. Med.* **363**, 1938–1948 (2010).
3. G. Dewson, P. J. A. Eichhorn, D. Komander, Deubiquitinases in cancer. *Nat. Rev. Cancer* **23**, 842–862 (2023).
4. V. Spataro, A. Buetti-Dinh, POH1/Rpn11/PSMD14: A journey from basic research in fission yeast to a prognostic marker and a druggable target in cancer cells. *Br. J. Cancer* **127**, 788–799 (2022).
5. Y. Liu, L. Zhang, B. Wang, Z. Yang, G. Xu, A. Ma, M. Tang, T. Jing, L. Wu, X. Xu, Y. Liu, Requirement for POH1 in differentiation and maintenance of regulatory T cells. *Cell Death Differ.* **26**, 751–762 (2019).
6. L. He, C. Yu, S. Qin, E. Zheng, X. Liu, Y. Liu, S. Yu, Y. Liu, X. Dou, Z. Shang, Y. Wang, Y. Wang, X. Zhou, B. Liu, Y. Zhong, Z. Liu, J. Lu, L. Sun, The proteasome component PSMD14 drives myelomagenesis through a histone deubiquitinase activity. *Mol. Cell* **83**, 4000–4016.e6 (2023).
7. S. M. Buckley, B. Aranda-Orgilles, A. Strikoudis, E. Apostolou, E. Loizou, K. Moran-Crusio, C. L. Farnsworth, A. A. Koller, R. Dasgupta, J. C. Silva, M. Stadtfeld, K. Hochedlinger, E. I. Chen, I. Aifantis, Regulation of pluripotency and cellular reprogramming by the ubiquitin-proteasome system. *Cell Stem Cell* **11**, 783–798 (2012).
8. Y. Wu, S. Jin, Q. Liu, Y. Zhang, L. Ma, Z. Zhao, S. Yang, Y. P. Li, J. Cui, Selective autophagy controls the stability of transcription factor IRF3 to balance type I interferon production and immune suppression. *Autophagy* **17**, 1379–1392 (2021).
9. L. R. Butler, R. M. Densham, J. Jia, A. J. Garvin, H. R. Stone, V. Shah, D. Weekes, F. Festy, J. Beesley, J. R. Morris, The proteasomal de-ubiquitinating enzyme POH1 promotes the double-strand DNA break response. *EMBO J.* **31**, 3918–3934 (2012).
10. B. Wang, A. Ma, L. Zhang, W. L. Jin, Y. Qian, G. Xu, B. Qiu, Z. Yang, Y. Liu, Q. Xia, Y. Liu, POH1 deubiquitylates and stabilizes E2F1 to promote tumour formation. *Nat. Commun.* **6**, 8704 (2015).
11. B. Wang, X. Xu, Z. Yang, L. Zhang, Y. Liu, A. Ma, G. Xu, M. Tang, T. Jing, L. Wu, Y. Liu, POH1 contributes to hyperactivation of TGF-β signaling and facilitates hepatocellular

carcinoma metastasis through deubiquitinating TGF-β receptors and caveolin-1. *EBioMedicine* **41**, 320–332 (2019).
12. C. Jing, X. Li, M. Zhou, S. Zhang, Q. Lai, D. Liu, B. Ye, L. Li, Y. Wu, H. Li, K. Yue, P. Chen, X. Yao, Y. Wu, Y. Duan, X. Wang, The PSMD14 inhibitor Thiolutin as a novel therapeutic approach for esophageal squamous cell carcinoma through facilitating SNAIL degradation. *Theranostics* **11**, 5847–5862 (2021).
13. P. Yang, X. Yang, D. Wang, H. Yang, Z. Li, C. Zhang, S. Zhang, J. Zhu, X. Li, P. Su, T. Zhuang, PSMD14 stabilizes estrogen signaling and facilitates breast cancer progression via deubiquitinating ERα. *Oncogene* **43**, 248–264 (2024).
14. D. Wiener, S. Schwartz, The epitranscriptome beyond m^6A. *Nat. Rev. Genet.* **22**, 119–131 (2021).
15. Y. Yang, P. J. Hsu, Y.-S. Chen, Y.-G. Yang, Dynamic transcriptomic m^6A decoration: Writers, erasers, readers and functions in RNA metabolism. *Cell Res.* **28**, 616–624 (2018).
16. Z. M. Zhu, F. C. Huo, J. Zhang, H. J. Shan, D. S. Pei, Crosstalk between m6A modification and alternative splicing during cancer progression. *Clin. Transl. Med.* **13**, e1460 (2023).
17. Z. Bi, Y. Liu, Y. Zhao, Y. Yao, R. Wu, Q. Liu, Y. Wang, X. Wang, A dynamic reversible RNA N^6-methyladenosine modification: Current status and perspectives. *J. Cell. Physiol.* **234**, 7948–7956 (2019).
18. Y. Wu, W. Zhao, Y. Liu, X. Tan, X. Li, Q. Zou, Z. Xiao, H. Xu, Y. Wang, X. Yang, Function of HNRNPC in breast cancer cells by controlling the dsRNA-induced interferon response. *EMBO J.* **37**, e99017 (2018).
19. M. Yan, L. Sun, J. Li, H. Yu, H. Lin, T. Yu, F. Zhao, M. Zhu, L. Liu, Q. Geng, H. Kong, H. Pan, M. Yao, RNA-binding protein KHSRP promotes tumor growth and metastasis in non-small cell lung cancer. *J. Exp. Clin. Cancer Res.* **38**, 478 (2019).
20. J. J. Chen, T. Z. Lu, T. Wang, W. H. Yan, F. Y. Zhong, X. H. Qu, X. C. Gong, J. G. Li, F. F. Tou, L. P. Jiang, X. J. Han, The m6A reader HNRNPC promotes glioma progression by enhancing the stability of IRAK1 mRNA through the MAPK pathway. *Cell Death Dis* **15**, 390 (2024).
21. Y. Zou, W. S. Henry, E. L. Ricq, E. T. Graham, V. V. Phadnis, P. Maretich, S. Paradkar, N. Boehnke, A. A. Deik, F. Reinhardt, J. K. Eaton, B. Ferguson, W. Wang, J. Fairman, H. R. Keys, V. Dančík, C. B. Clish, P. A. Clemons, P. T. Hammond, L. A. Boyer, R. A. Weinberg, S. L. Schreiber, Plasticity of ether lipids promotes ferroptosis susceptibility and evasion. *Nature* **585**, 603–608 (2020).
22. X. Chen, R. Kang, G. Kroemer, D. Tang, Broadening horizons: The role of ferroptosis in cancer. *Nat. Rev. Clin. Oncol.* **18**, 280–296 (2021).
23. J. Y. Lee, M. Nam, H. Y. Son, K. Hyun, S. Y. Jang, J. W. Kim, M. W. Kim, Y. Jung, E. Jang, S. J. Yoon, J. Kim, J. Kim, J. Seo, J. K. Min, K. J. Oh, B. S. Han, W. K. Kim, K. H. Bae, J. Song, J. Kim, Y. M. Huh, G. S. Hwang, E. W. Lee, S. C. Lee, Polyunsaturated fatty acid biosynthesis pathway determines ferroptosis sensitivity in gastric cancer. *Proc. Natl. Acad. Sci. U.S.A.* **117**, 32433–32442 (2020).
24. C. Glaser, J. Heinrich, B. Koletzko, Role of *FADS1* and *FADS2* polymorphisms in polyunsaturated fatty acid metabolism. *Metabolism* **59**, 993–999 (2010).
25. S. Shen, J. W. Park, Z. X. Lu, L. Lin, M. D. Henry, Y. N. Wu, Q. Zhou, Y. Xing, rMATS: Robust and flexible detection of differential alternative splicing from replicate RNA-seq data. *Proc. Natl. Acad. Sci. U.S.A.* **111**, E5593–E5601 (2014).
26. C. R. Alarcón, H. Goodarzi, H. Lee, X. Liu, S. Tavazoie, S. F. Tavazoie, HNRNPA2B1 is a mediator of m^6A-dependent nuclear RNA processing events. *Cell* **162**, 1299–1308 (2015).
27. N. Liu, Q. Dai, G. Zheng, C. He, M. Parisien, T. Pan, N^6-methyladenosine-dependent RNA structural switches regulate RNA-protein interactions. *Nature* **518**, 560–564 (2015).
28. W. Xiao, S. Adhikari, U. Dahal, Y.-S. Chen, Y.-J. Hao, B.-F. Sun, H.-Y. Sun, A. Li, X.-L. Ping, W.-Y. Lai, X. Wang, H.-L. Ma, C.-M. Huang, Y. Yang, N. Huang, G.-B. Jiang, H.-L. Wang, Q. Zhou, X.-J. Wang, Y.-L. Zhao, Y.-G. Yang, Nuclear m^6A reader YTHDC1 regulates mRNA splicing. *Mol. Cell* **61**, 507–519 (2016).
29. R. Zhao, L. Tian, B. Zhao, Y. Sun, J. Cao, K. Chen, F. Li, M. Li, D. Shang, M. Liu, FADS1 promotes the progression of laryngeal squamous cell carcinoma through activating AKT/mTOR signaling. *Cell Death Dis.* **11**, 272 (2020).
30. C. Berndt, H. Alborzinia, V. S. Amen, S. Ayton, U. Barayeu, A. Bartelt, H. Bayir, C. M. Bebber, K. Birsoy, J. P. Böttcher, S. Brabletz, T. Brabletz, A. R. Brown, B. Brüne, G. Bulli, A. Bruneau, Q. Chen, G. M. DeNicola, T. P. Dick, A. Distéfano, S. J. Dixon, J. B. Engler, J. E.-v. Bieren, M. Fedorova, J. P. Friedmann Angeli, M. A. Friese, D. C. Fuhrmann, A. J. García-Sáez, K. Garbowicz, M. Götz, W. Gu, L. Hammerich, B. Hassannia, X. Jiang, A. Jeridi, Y. P. Kang, V. E. Kagan, D. B. Konrad, S. Kotschi, P. Lei, M. L. Tertre, S. Lev, D. Liang, A. Linkermann, C. Lohr, S. Lorenz, T. Luedde, A. Methner, B. Michalke, A. V. Milton, J. Min, E. Mishima, S. Müller, H. Motohashi, M. U. Muckenthaler, S. Murakami, J. A. Olzmann, G. Pagnussat, Z. Pan, T. Papagiannakopoulos, L. P. Puentes, D. A. Pratt, B. Proneth, L. Ramsauer, R. Rodriguez, Y. Saito, F. Schmidt, C. Schmitt, A. Schulze, A. Schwab, A. Schwantes, M. Soula, B. Spitzlberger, B. R. Stockwell, L. Thewes, O. Thorn-Seshold, S. Toyokuni, W. Tonnus, A. Trumpp, P. Vandenabeele, T. V. Berghe, V. Venkataramani, F. C. E. Vogel, S. von Karstedt, F. Wang, F. Westermann, C. Wientjens, C. Wilhelm, M. Wölk, K. Wu, X. Yang, F. Yu, Y. Zou, M. Conrad, Ferroptosis in health and disease. *Redox Biol.* **75**, 103211 (2024).
31. J. Lv, S. Zhang, H. Wu, J. Lu, Y. Lu, F. Wang, W. Zhao, P. Zhan, J. Lu, Q. Fang, C. Xie, Z. Yin, Deubiquitinase PSMD14 enhances hepatocellular carcinoma growth and metastasis by stabilizing GRB2. *Cancer Lett.* **469**, 22–34 (2020).
32. E. M. Cooper, C. Cutcliffe, T. Z. Kristiansen, A. Pandey, C. M. Pickart, R. E. Cohen, K63-specific deubiquitination by two JAMM/MPN+ complexes: BRISC-associated Brcc36 and proteasomal Poh1. *EMBO J.* **28**, 621–631 (2009).
33. Y. Wu, A. Li, C. Chen, Z. Fang, L. Chen, X. Zheng, Biological function and research progress of N^6-methyladenosine binding protein heterogeneous nuclear ribonucleoprotein A2B1 in human cancers. *Front. Oncol.* **13**, 1229168 (2023).
34. H. Fischl, J. Neve, Z. Wang, R. Patel, A. Louey, B. Tian, A. Furger, hnRNPC regulates cancer-specific alternative cleavage and polyadenylation profiles. *Nucleic Acids Res.* **47**, 7580–7591 (2019).
35. W. Zhu, J. Wang, X. Liu, Y. Xu, R. Zhai, J. Zhang, M. Wang, M. Wang, L. Liu, lncRNA CYTOR promotes aberrant glycolysis and mitochondrial respiration via HNRNPC-mediated ZEB1 stabilization in oral squamous cell carcinoma. *Cell Death Dis.* **13**, 703 (2022).
36. F. Martino, N. M. Varadarajan, A. R. Perestrelo, V. Hejret, H. Durikova, D. Vukic, V. Horvath, F. Cavalieri, F. Caruso, W. S. Albihlal, A. P. Gerber, M. A. O'Connell, S. Vanacova, S. Pagliari, G. Forte, The mechanical regulation of RNA binding protein hnRNPC in the failing heart. *Sci. Transl. Med.* **14**, eabo5715 (2022).
37. Y. Cai, T. Lyu, H. Li, C. Liu, K. Xie, L. Xu, W. Li, H. Liu, J. Zhu, Y. Lyu, X. Feng, T. Lan, J. Yang, H. Wu, LncRNA CEBPA-DT promotes liver cancer metastasis through DDR2/β-catenin activation via interacting with hnRNPC. *J. Exp. Clin. Cancer Res.* **41**, 335 (2022).
38. S. L. Sarbanes, J. Le Pen, C. M. Rice, Friend and foe, HNRNPC takes on immunostimulatory RNAs in breast cancer cells. *EMBO J.* **37**, e100923 (2018).
39. C. Cretu, J. Schmitzová, A. Ponce-Salvatierra, O. Dybkov, E. I. De Laurentiis, K. Sharma, C. L. Will, H. Urlaub, R. Lührmann, V. Pena, Molecular architecture of SF3b and structural consequences of its cancer-related mutations. *Mol. Cell* **64**, 307–319 (2016).
40. C. Han, A. Khodadadi-Jamayran, A. H. Lorch, Q. Jin, V. Serafin, P. Zhu, Y. Politanska, L. Sun, B. T. Gutierrez-Diaz, M. V. Pryzhkova, H. Abdala-Valencia, E. T. Bartom, B. Buldini, G. Basso, S. E. Velu, K. Sarma, B. B. Mattamana, B. K. Cho, R. C. Obeng, Y. A. Goo, P. W. Jordan, A. Tsirigos, Y. Zhou, P. Ntziachristos, SF3B1 homeostasis is critical for survival and therapeutic response in T cell leukemia. *Sci. Adv.* **8**, eabj8357 (2022).
41. T. Xu, X. Li, W. Zhao, X. Wang, L. Jin, Z. Feng, H. Li, M. Zhang, Y. Tian, G. Hu, Y. Yue, X. Dai, C. Shan, W. Zhang, C. Zhang, Y. Zhang, SF3B3-regulated mTOR alternative splicing promotes colorectal cancer progression and metastasis. *J. Exp. Clin. Cancer Res.* **43**, 126 (2024).
42. N. Kawamura, K. Nimura, K. Saga, A. Ishibashi, K. Kitamura, H. Nagano, Y. Yoshikawa, K. Ishida, N. Nonomura, M. Arisawa, J. Luo, Y. Kaneda, SF3B2-mediated RNA splicing drives human prostate cancer progression. *Cancer Res.* **79**, 5204–5217 (2019).
43. F. Xiong, S. Li, SF3b4: A versatile player in eukaryotic cells. *Front. Cell Dev. Biol.* **8**, 14 (2020).
44. G. Heravi, H. Jang, X. Wang, Z. Long, Z. Peng, S. Kim, W. Liu, Fatty acid desaturase 1 (FADS1) is a cancer marker for patient survival and a potential novel target for precision cancer treatment. *Front. Oncol.* **12**, 942798 (2022).
45. C. Xu, L. Gu, L. Hu, C. Jiang, Q. Li, L. Sun, H. Zhou, Y. Liu, H. Xue, J. Li, Z. Zhang, X. Zhang, Q. Xu, FADS1-arachidonic acid axis enhances arachidonic acid metabolism by altering intestinal microecology in colorectal cancer. *Nat. Commun.* **14**, 2042 (2023).
46. P. Liao, W. Wang, W. Wang, I. Kryczek, X. Li, Y. Bian, A. Sell, S. Wei, S. Grove, J. K. Johnson, P. D. Kennedy, M. Gijón, Y. M. Shah, W. Zou, $CD8^+$ T cells and fatty acids orchestrate tumor ferroptosis and immunity via ACSL4. *Cancer Cell* **40**, 365–378.e6 (2022).
47. Y. Yu, H. Deng, W. Wang, S. Xiao, R. Zheng, L. Lv, H. Wang, J. Chen, B. Zhang, LRPPRC promotes glycolysis by stabilising LDHA mRNA and its knockdown plus glutamine inhibitor induces synthetic lethality via m^6A modification in triple-negative breast cancer. *Clin. Transl. Med.* **14**, e1583 (2024).

Acknowledgments: We thank LetPub (www.letpub.com) for its linguistic assistance during the preparation of this manuscript. **Funding:** The work was supported, in whole or in part, by the National Natural Science Foundation of China (82203813 to H.C, 82303861 to J.H., 82303124 to W.W., 82373055 to L.L., 82403213 to Y.Y., and 82373144 to C. Liu), the High-level Talents Program of Hainan Province Natural Science Foundation (823RC594 to H.C.), and the Hubei Provincial Key Research and Development Program (2023BCB011 to C. Liu and 2024BE020 to L.L.). **Author contributions:** Conceptualization: L.L., C. Liu, E.Z., and Y.Y. Methodology: L.L., Y.Y., H.C., P.Z., E.Z., and W.W. Investigation: L.L., H.C., Y.Y., and H.L. Visualization: L.L., Y.Y., and Z.X. Supervision: L.L., C. Liu, C. Lu, and H.C. Project administration: L.L. and C. Lu. Formal analysis: L.L., P.Z., Z.X., E.Z., and H.L. Validation: L.L., P.Z., and H.L. Software: L.L., P.Z., and W.W. Resources: L.L., Z.X., and H.L. Data curation: L.L., Z.X., and H.L. Funding acquisition: L.L., H.C., C. Liu, and J.H. Writing—original draft: L.L., Y.Y., and J.H. Writing—review and editing: Y.Y., H.C., E.Z., L.L., and C. Liu. **Competing interests:** The authors declare that they have no competing interests. **Data and materials availability:** All data needed to evaluate the conclusions in the paper are present in the paper and/or the Supplementary Materials.

Submitted 1 July 2024
Accepted 3 April 2025
Published 9 May 2025
10.1126/sciadv.adr3173